A&A 390, 891–915 (2002)
DOI: 10.1051/0004-6361:20020759

Astronomy & Astrophysics

Massive (?) starburst hosts of blue compact galaxies (BCGs)

Optical/near-IR observations of 4 BCGs and their companions⋆

N. Bergvall[1] and G. Östlin[2]

[1] Dept. of Astronomy and Space Physics, Box 515, S-75120 Uppsala, Sweden
e-mail: nils.bergvall@astro.uu.se
[2] Stockholm Observatory, SCFAB, SE-106 91 Stockholm, Sweden
e-mail: ostlin@astro.su.se

Received 29 November 2001 / Accepted 15 May 2002

Abstract. We present optical spectroscopy and deep optical/near-IR photometry of 4 luminous metal-poor blue compact galaxies (BCGs) and two of their companions. With the aid of spectral evolutionary models (SEMs) and structural parameters derived from the surface photometry we discuss the properties of the central starbursts and the halo populations of the galaxies. Special attention is paid to the effects of dust, chemical inhomogeneities and contamination of nebular emission to the halo light. The optical/near-IR colour index profiles show a sharp distinction between the starburst and the host. The hosts have luminosity profiles characteristic of massive ellipticals and remarkably red colours, typical of a relatively *metal-rich* stellar population of *old age*. These properties are in conflict with the relatively low luminosities. The situation can best be explained if the hosts have an unusually large amount of dark matter that can hinder the outflow of metals from the system.The indicated difference in metallicity between the halo and the young starburst disproves the recurrent burst scenario and supports different origins of the two populations. We conclude that these BCGs are undergoing mergers between early type galaxies/thick disks and gas-rich galaxies or intergalactic HI clouds, in many respects reminiscent of a retarded formation of massive ellipticals.

Key words. galaxies: evolution – galaxies: formation – galaxies: starburst – galaxies: dwarfs

1. Introduction

1.1. General comments

Blue compact galaxies (BCGs), sometimes called HII galaxies, are characterized by globally active star formation, low chemical abundances (e.g. Searle & Sargent 1972; Marconi et al. 1994; Kunth & Östlin 2000; Masegosa et al. 1994) and relatively high HI masses (Gordon & Gottesman 1981; Thuan & Martin 1981; Staveley-Smith et al. 1992). These are properties normally associated with young galaxies and indeed there have been claims from time to time (Searle & Sargent 1972; Thuan & Izotov 1997) that some BCGs may be truly young systems. But the most important aspect today is that BCGs constitute an important link to the high redshift universe and the early epoch of galaxy formation.

Observations (e.g. Lilly et al. 1999; Le Fèvre et al. 2000) show that mergers between galaxies are of major importance for the buildup of galaxies at high redshifts. The BCGs and their progenitors (HI clouds, LSB galaxies or other gas-rich dwarfs) that contribute fuel for the starburst may therefore be regarded as the local analogues of the distant subunits participating in the early merger processes. While starbursts of massive galaxies are rare, those induced by mergers of galaxies of intermediate mass may produce a major fraction of the metals observed in the intergalactic medium (IGM) during the buildup processes at high redshifts. A necessary requirement is that the energy input from the exploding supernovae is sufficiently large to overcome the gravitation. This requires masses of the galaxies not much in excess of typical luminous BCGs, making this type of galaxy interesting also from this point of view.

For a better understanding of the star formation processes we want to disentangle the different phases involved in the formation of a BCG by identifying stellar populations and galaxy morphologies of components from different epochs. We also want to know under what conditions a starburst can be triggered. Are the conditions set by external conditions, like the orbital properties of infalling clouds, or is a specific type of galaxy needed to host the burst?

1.2. Ages of BCGs and the youth hypothesis

From studies of the central starburst region of BCGs, it is very difficult to rule out that the galaxy is young since the starburst population easily outshines even a relatively massive population of old stars. Therefore, some investigations have focused

Send offprint requests to: N. Bergvall,
e-mail: nils.bergvall@astro.uu.se

⋆ Based on observations collected at the European Southern Observatory, La Silla, Chile.

on the halos of BCGs, where the starburst influence is assumed to be milder. Most BCGs show a regular halo (e.g. Loose & Thuan 1986). Already this fact is a strong argument in favour of a fairly old age because the relaxation time of a system of stars of a typical size of a few kpc is larger than a few times 10^8 yr. But a regular halo can be formed on a shorter time scale if the medium is viscous. The light may be due to nebular emission, a "Strömgrensphere" formed by the starburst in the centre. We will elaborate on this a bit further in Sect. 6. If so, the stellar component whose formation may be much delayed relative to the gaseous disk of a protogalaxy, may be quite young.

One of the most debated young galaxy candidates is IZw18, which belongs to the blue compact dwarfs (BCDs). These are galaxies in the mass range 10^7–10^9 $\mathcal{M}_\odot$, having relatively low luminosities ($M_B > -17$). IZw18 has unique properties in this category, in particular its record-low oxygen abundance of approximately 1/50 of the solar value (e.g. Alloin et al. 1978; Izotov & Thuan 1999). There are however reasons to suspect that winds from massive stars and supernovae in low-mass galaxies may expel the gas and lower the chemical abundances in which case the youth signature may not be more than an artifact (e.g. McLow & Ferarra 1999; Lequeux et al 1995; Martin 1996). It is also a bit difficult to cope the relatively low $\mathcal{M}(\mathrm{HI})/M_B \sim 1$ in IZw18 (Thuan & Martin 1981) with a recently born galaxy. As we show below (Fig. 1), already a "simple" set of data such as the integrated near-IR colours indicate that this is an old galaxy. Recent investigations of deep colour-magnitude diagrams of IZw18, in the optical by Aloisi et al. (1999) and in the near IR by Östlin (2000), show that the galaxy contains a population of evolved red stars, indicating an age in excess of 1 Gyr. Among other young galaxy candidates discussed in the literature (Bergvall & Jörsäter 1988) is one of the targets in this project, ESO 400-G43, but as we will show below this galaxy also seems to contain old stars. Another debated young galaxy candidate is SBS0335-052 (Thuan & Izotov 1997; Östlin & Kunth 2001).

Near-IR photometry has proven to be quite powerful in deriving information about the star formation history in galaxies that are dominated by starbursts and seems to support the idea that BCGs are old (e.g. Bergvall et al. 1999; Doublier et al. 2001). Then the interesting question remains what kind of galaxy or galaxies the precursor(s) and the successors could be. Several different scenarios for the ignition of the burst and the types of galaxies involved have been discussed in the literature (e.g. Searle & Sargent 1972; Thuan & Seitzer 1979; Thuan & Martin 1981; Staveley-Smith et al. 1992; Taylor et al. 1994; Telles & Terlevich 1995; Papaderos et al. 1996). One should be careful not to consider all BCDs as starburst galaxies, as is the commonly accepted view. In fact Sage et al. (1992) find that most BCDs are not more efficient in converting gas into stars than are normal spiral galaxies. They appear to be bursting only when compared to other gas-rich dwarfs where the normal star formation rate (SFR) is lower than in massive gas-rich galaxies. It is important to keep in mind that the class of BCGs is quite heterogeneous (Kunth et al. 1988; Kunth & Östlin 2000) and may include objects with different histories. Some galaxies called BCGs by some groups are definitely not BCGs since they easily fit into the extended Hubble classification towards late type disks or normal irregulars (Sandage & Binggeli 1984).

In this work we are dealing with galaxies that have extremely high *star formation efficiencies* (SFE). With SFE we mean the timescale of gas consumption in a closed box scenario, and a short timescale is equal to a high SFE. From our spectral evolutionary models (SEMs), assuming a Salpeter mass function (1958) and a mass range of 0.1–120 $\mathcal{M}_\odot$ we find a SFR of $\sim$10 $\mathcal{M}_\odot$ yr^{-1} for a burst with M_B between -19 and -20. Assuming a gas mass of 10^9 $\mathcal{M}_\odot$, which is typical for our sample, we thus obtain a maximum lifetime of the burst of not more than a few times 10^8 yr, allowing for a modest fading of the burst. Thus, if no fresh gas is supplied the starburst will be a transient phenomenon during which the properties of the galaxy will change from what it was before, allowing a morphological metamorphosis to take place. Based on photometric properties, globular cluster properties, HI masses, kinematics and chemical abundances (e.g. Bergvall et al. 1998; Östlin et al. 1998, 2001) we have claimed that a large fraction of luminous BCGs may form from mergers involving massive gas rich low surface brightness galaxies or gas clouds and possibly early type dwarfs. More support in favour of this will be presented below as we discuss the properties of 4 such massive BCGs. The relationships between HI, chemical abundances and photometric properties will be discussed in a paper now in preparation.

1.3. Outflows of enriched gas

As noted below, we have observational support for bipolar outflows from the BCGs discussed here. An interesting question to ask is under what conditions and to what extent the metals in these outflows can reach the escape velocity and be expelled into the ambient intergalactic medium (IGM) and how much of the metals observed in Lyα systems and the hot intracluster gas in rich galaxy clusters that can be explained this way. Outflows will also open channels in the gaseous halos, making it easier for Ly-continuum photons to escape. Starburst dwarfs may therefore contribute significantly to the reionisation of the IGM after recombination.

McLow & Ferarra (1999) argue that galaxies with masses exceeding 5×10^7 $\mathcal{M}_\odot$ (less than a few % of the masses of our targets) will retain most of their gas indefinitely, while a large fraction of the metals may be lost. If a bottom-up scenario is relevant for early galaxy formation it could be argued that most of the pollution of the IGM in the early days were caused by outflows from starburst dwarfs, similar to the local BCGs. These important topics deserve a thorough investigation but is not the prime goal of this paper. Still, as we illustrate below, we have to consider the possibility that the outflows influence the properties of the halo through polluting the light with emission from ionised gas of low temperature.

1.4. Near-IR properties of BCGs in general

Before entering into the results of this paper, it is enlightening to have a look at the integrated near-IR properties of BCGs in

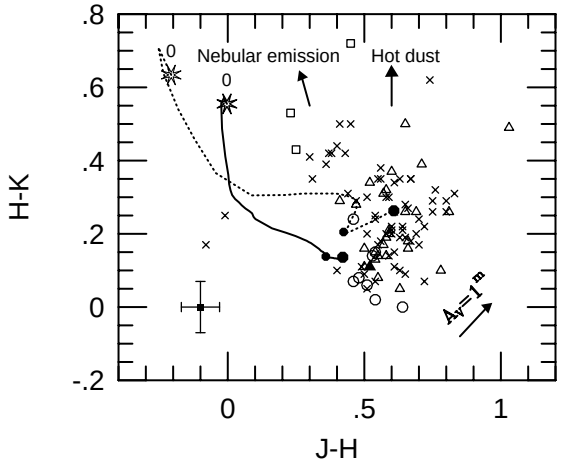

Fig. 1. The $J-H/H-K$ two colour diagram of BCGs (crosses), luminous irregulars (triangles), HII regions (squares) and dE:s (circles) obtained from Bergvall & Olofsson (1986), Hunter & Gallagher (1985), James (1994) and Thuan (1983). The predicted evolution (Zackrisson et al. 2001) of a star forming galaxy with a Salpeter mass function, an e-folding star formation decay rate of 14 Gyr and two different metallicities (20% solar, solid line; twice solar, dotted line) are also displayed. The evolution starts at the star marked 0 and ends at the large black dot, corresponding to an age of 14.5 Gyr. The position at 1 Gyr is marked with a smaller black dot. The effect of dust reddening and emission are indicated by arrows but note that the nebular emission has been included in the model. The filled triangle at $J-H=0.5$, $H-K=0.1$ is IZw18. Typical mean errors are indicated on the lower left side.

general. In Fig. 1 we show the $J-H$ vs. $H-K$ diagram of BCGs, dIs and dEs with available photometry from the literature. In the diagram we have also indicated the evolution of a star forming galaxy with a Salpeter IMF and an exponentially decaying SFR (e-folding time 14 Gyr). Two tracks are shown, representing different metallicities (0.2 $Z_{\odot}$ and 2 $Z_{\odot}$). The galaxy positions are quite dispersed in the diagram. As mentioned above, BCGs in general is a very heterogeneous group of galaxies, composed of subgroups with different evolutionary histories. Despite the spread in Fig. 1 it is obvious that most, if not all, galaxies contain old stars.

Some spread may be due to varying data quality, and differences in metallicity and extinction. However, even when these effects are taken into account, it seems as if the observed distribution is shifted towards slightly redder $J-H$. The difference can be reduced with 0.1 mag if we assume that the star formation rate declines faster so that the influence from young stars becomes less important. In the cases where the galaxy contains an old population of stars and the starburst is not so strong we would expect that the old stars dominate in the infrared. This is indeed where most of the BCGs are found in the diagram. Only a few BCGs with strong starbursts are located along the evolutionary track with low ages.

1.5. Target selection

In this paper we focus on luminous BCGs. Such BCGs are likely to have deeper central potential wells and therefore should be more capable retaining the gas than the true dwarfs. In less massive galaxies the metals may be quickly diluted due to winds from high mass stars and could therefore mimic a truly young galaxy. The massive BCGs are more suited for dynamical mass determinations and they are massive enough to show similarities with normal disk galaxies in formation.

There is no commonly-accepted definition of a blue compact galaxy. We have simply chosen luminous galaxies with high central surface brightnesses, blue colours and low chemical abundances from the list of Bergvall & Olofsson (1986). For quite some time we have observed a number of such galaxies and chosen a few for a more detailed study. We have selected those that have metallicities <15% of the solar values, although none of them as low as IZw18. In view of the discussions concerning the possible existence of young galaxies in the local universe we also as a second criterion rejected objects that showed regularity in the central regions. This was done after inspection of CCD images (mostly unpublished data) obtained with the ESO 1.5m telescope of about 15 galaxies from the Bergvall and Olofsson list. Here we discuss the properties of four of these and two of their companions. We hope that by making a more detailed study as presented here and in accompanying papers we can contribute to improving the classification methods for this type of BCG. Throughout this paper we will assume a Hubble parameter of $H_0 = 75$ km s^{-1} Mpc^{-1}.

2. Observations and reductions

2.1. Spectroscopy

Spectroscopy was carried out at ESO, La Silla, in 1983 and 1984 using the IDS at the ESO 1.5-m and 3.6-m telescope and in October 8-10 1986 using the EFOSC1 spectrograph/camera at the 3.6-m telescope, equipped with an RCA CCD chip. In the first case we used an aperture of $4'' \times 4''$ and a spectral resolution of 12 Å. The spectral coverage was ~3600–7700 Å. The aperture was centered on the maximum intensity in the visual of the central region of the galaxies. The weather conditions were fair. EFOSC1 was used with the B300 and O150 grisms, with a wavelength coverage of 3600–7000 and 3600–5590 Å and a dispersion of 230 and 130 Åmm^{-1} respectively. Here we will only discuss some of the results obtained with the B300 grism. We used a slit size of 2 arcsec. It gives a spectral resolution of ~15 Å. The seeing conditions were poor with a mean seeing of ~2 arcsec. At both occasions standard stars were observed each night to derive the response curves. La Silla mean extinction was adopted when correcting to zero airmass. Dome flatfields were obtained with a Tungsten lamp. The spectra were reduced using the ESO MIDAS software. Final measurements of the spectra were made using software developed in Uppsala. When measuring line strengths, the continuum was defined with a linear approximation and the line with a gaussian approximation. The Hα line was derived from a decomposition of two Gaussian approximations of the Hα line and the [NII]λ6584 line.

Table 1. Log of optical imagery.

ESO id.	RA_{1950}	$Decl._{1950}$	Year	Telescope	Filters and integration times (minutes)	Seeing (arcsec)
338-04 (Tol 1924-416)	19 24 29.0	−41 40 36	1995	NTT	Hα (10), Hα-continuum (33)	1
			1997	NTT	B(5), V(15), R(15), I(30)	1
338-04b	19 24 03	−41 45 00	1997	NTT	V(5), I(5)	1
350-38 (Haro 11)	00 34 25.7	−33 49 49	1984	2.2 m	B(25), V(15), Gunn i(20)	<1
			1988	1.5D	Gunn r(90)	1
			1989	1.5D	Hα (20)	1
400-43	20 34 31.0	−35 39 42	1984	2.2 m	Hα (60)	1
			1989	2.2 m	B (30), Gunn r (90), Hα (90)	<1
			1995	NTT	Hα (30), Hα-continuum (55)	1.5
400-43b	20 34 31.0	−35 39 42	1989	2.2 m	B (5), Gunn r (5)	<1
480-12	02 52 32.8	−25 18 49	1984	2.2 m	B(25), V(20), Hα (20)	1
			1989	2.2 m	B (30), V (20), Gunn r (45)	<1

Table 2. Log of near-IR imagery.

ESO id.	Integration time (seconds)		
	J	H	K'
338-04	1000	2000	3000
338-04b	1000	2000	3000
358-38	1000	3000	4000
400-43	2000	4000	5000
400-43b	1000	1000	2000
480-12	1000	1000	2000

2.2. Optical photometry

Broad and narrowband optical images were obtained at five occasions in the period 1983–1997. The broadband filters *UBVRI* were in the Cousins system and *r* and *i* filters also in the Gunn-Thuan system. Narrowband images were obtained in Hα and Hβ. The bandwidths of these filters were ∼70 Å. The central wavelengths coincide roughly with the central rest wavelengths of the lines. Standard stars were obtained during each night. Colour transformations between Cousins and the Gunn-Thuan systems were carried out simply by comparing images of the same objects obtained at different occasions in the two different systems and making the zeropoints agree with the Cousins system. The colour dependence was thus not taken into account. From previous calibrations of colour transformation equations (Rönnback & Bergvall 1994) we estimate that the mean errors in the colours due to this approximation are less than a few 0.01 mag. The major conclusions are based on data unaffected by this. Mean extinction coefficients for La Silla were used in the photometric corrections to zero airmass. The weather conditions for photometry were average-excellent. The observations are summarized in Table 1.

2.3. Near infrared photometry

JHK′ observations were carried out with the near-IR camera IRAC2 at the ESO 2.2-m telescope, equipped with a 256×256 $pixel^2$ NICMOS detector in August 1993. Of the available field lenses we chose to work with the C lens, which gives a pixel size of 0.49 arcsec and a field size of 2 arcmin. The weather conditions were good with a seeing of 1–1.5 arcsec. At least 3 different standard stars each night were used for calibration. For flatfield corrections we used a superflat constructed from about 10 object frames where the target galaxy had been shifted to different positions on the chip between the integrations. A list of integration times in each filter is found in Table 2.

2.4. Luminosity profiles

Since much of the discussion below focuses on the shape of the profiles at the faintest surface brightness levels, is it crucial to have full control of the error estimates that determine the reliability of the structure parameters. We have good control of the reductions of the optical images, since the field size is considerably larger than the galaxies. In the near-IR images the field size is smaller and the sky background is noisier which makes the sky subtraction more unreliable. We are aware of these problems when we analyze the fainter isophotes in the near-IR profiles.

The profiles were derived in the following way. Firstly we removed hot pixels in the images. This is automatically done when we stack the images in cases where we have several exposures. In other cases, where only one exposure is available, we used the command filter/cosmic in MIDAS. This procedure efficiently and highly selectively removes hot pixels and nearby correlated pixels. Secondly, we approximated the sky background by fitting the sky brightness distribution, measured by integrating in small boxes placed in regions which appeared empty of stars, to a 1–3 degree polynomial. We used a degree

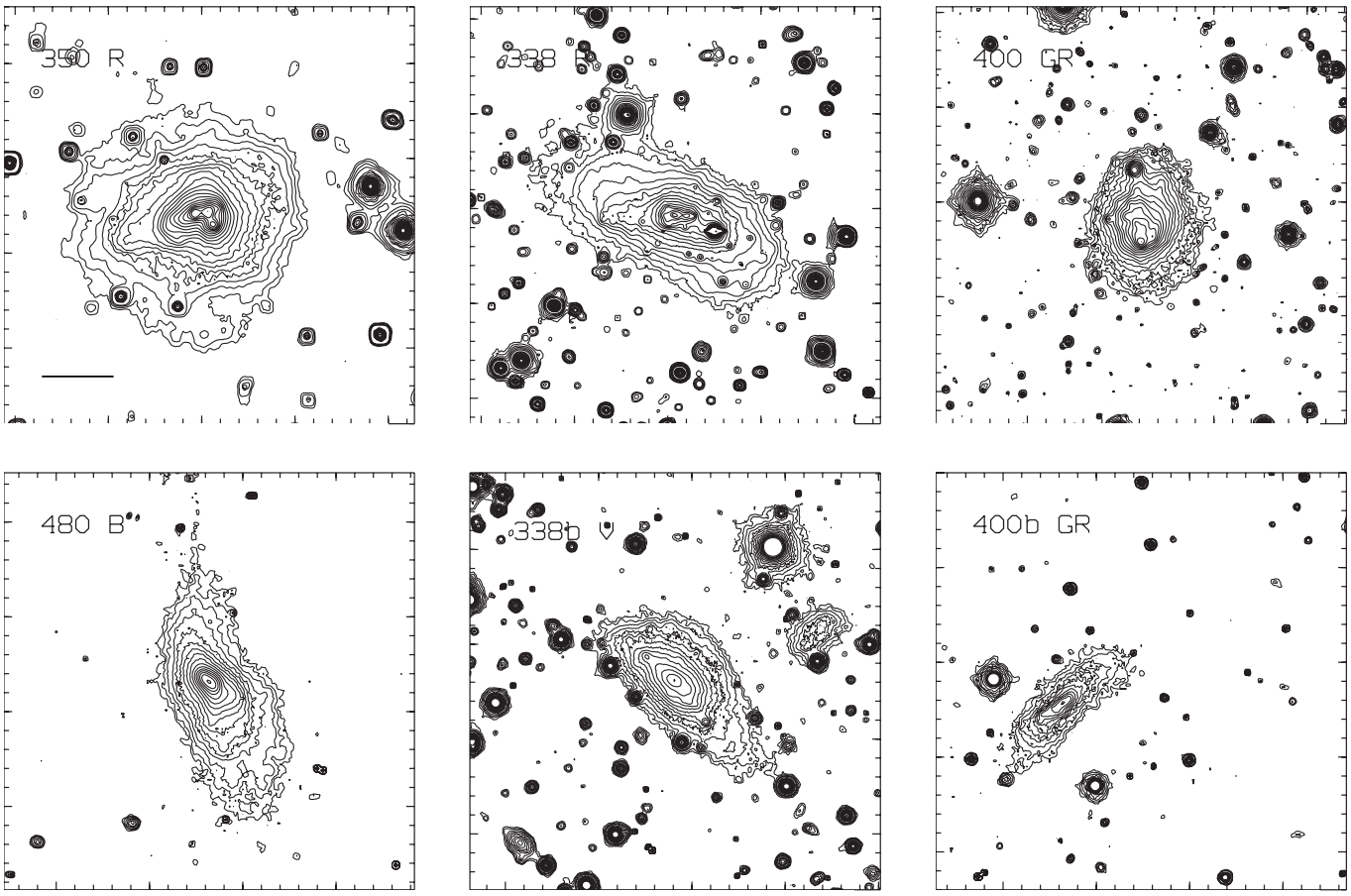

Fig. 2. Optical broadband images of ESO 338-IG04 (Tol 1924-426), 338-IG04b, 350-IG38 (Haro 11), 400-G43, 400-G43b and 480-IG12. The filters, indicated after the abbreviated object name on top of the images, are in the Bessel system except those marked GR which is the *r* filter in the Thuan-Gunn system. A median 3×3 pixel filter was applied on the lower flux levels. The steps between the isophotes are constant on a logarithmic scale arbitrarily chosen for each galaxy such that the details are enhanced. North is up, east is to the left. The field size is 95″ ×95″.

as low as possible so that the residuals looked acceptable. To estimate the uncertainty in the final sky level, we calculated the median sky value in each box and the standard deviation of the median values for all the boxes. We use this as a measure of the error of the zeropoint of the sky level. This normally dominates the error sources of the surface luminosities at the faintest isophotes. To further check the stability of the result we in a few cases remade the sky subtraction. Next step was to remove all stars and galaxies in the field by hand and flag these regions not to be included in the following derivation of the profile. Then we determined the centre, inclination and position angle of the outermost profiles and integrated the light in elliptical strips with a width of 1 pixel based on these parameters. We want to point out already here that the profiles displayed in the diagrams presented below have also been corrected for inclination assuming an infinitely thin disk.

3. Spectral evolutionary models

The spectral evolutionary models (SEMs) we use in the discussions regarding the stellar content come from an in-house model by Zackrisson et al. (2001), PEGASE2 (Fioc & Rocca-Volmerange 2000) and the model from Worthey (1994). In the spectral analysis we also use a model by Bergvall (Bergvall & Rönnback 1995). The Zackrisson et al. models are based on stellar evolutionary tracks with the major contribution from the Geneva group, synthetic stellar spectra from the compilation by Lejeune et al. (1998) and a nebular component obtained from the Cloudy model (Ferland 1996). In Sect. 6 we use these models to compare between the predicted and observed broadband colours of the halo. We show below that the contribution from ionised gas to the halo light is fairly small, also in the *R* band, and that the uncertainties due to the nebular emission are not significantly affecting the derived results. This facilitates the analysis and improves the reliability of the method when used for information about the star formation history.

It is important to clarify that we do not intend to discuss the ionisation structure, sources, metallicities and so on in any detail here but rather the reverse – we are content with the situation that we do not need to worry about this component in the halo. If we had the ambition to discuss the star formation history of the central burst the situation would be much more complicated due to the unknown effects of dust, subcondensations in the gas and Lyman photon leakage, just to mention a few problems.

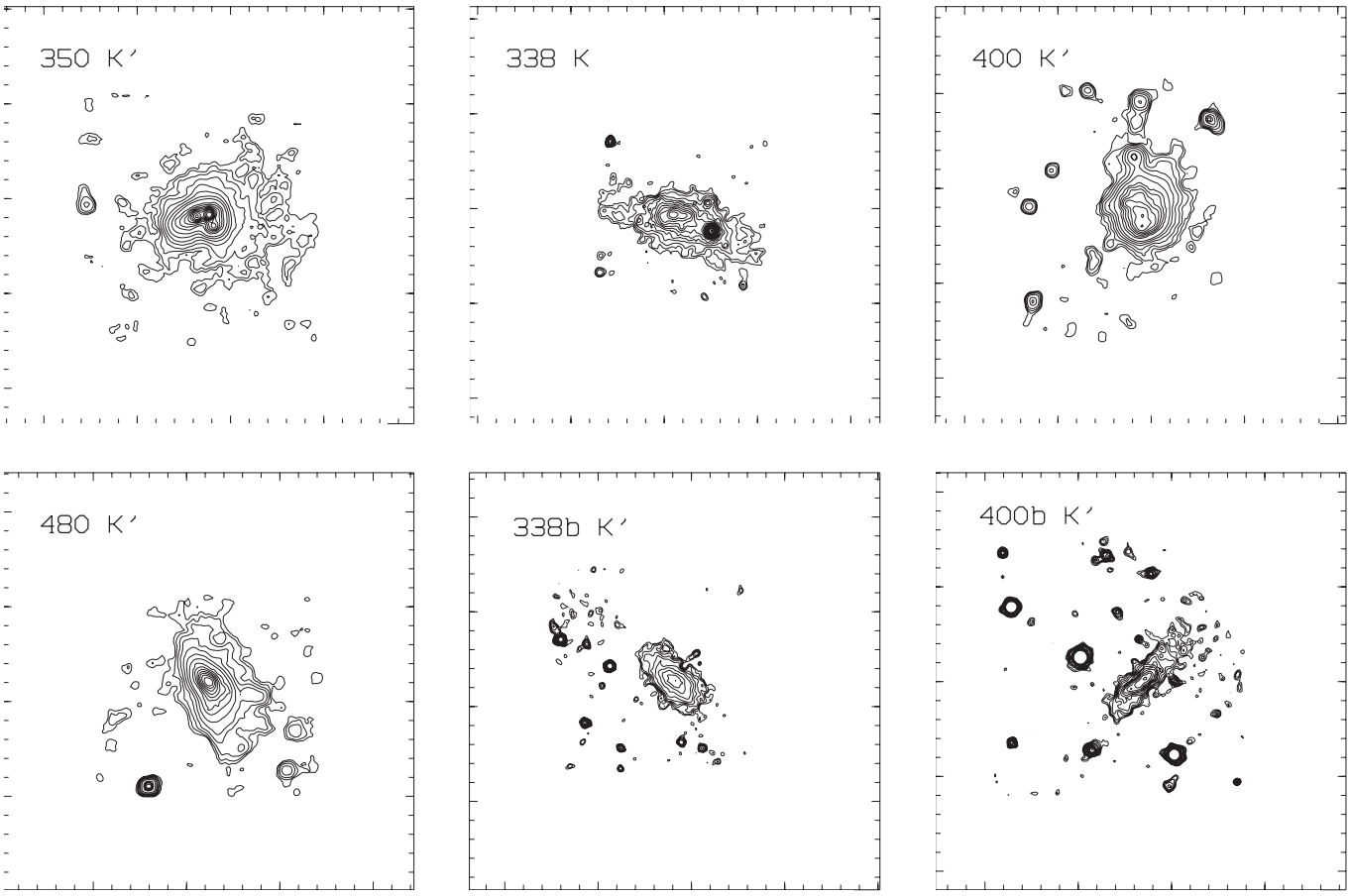

Fig. 3. Johnson K' broadband images of the programme galaxies. The steps between the isophotes are constant on a logarithmic scale arbitrarily chosen for each galaxy such that the details are enhanced. North is up, east is to the left. The field size is $95'' \times 95''$.

Table 3. Integrated surface photometry. The table lists the B magnitude and broadband colours obtained from integrating in elliptic rings of position angle PA (degrees), inclination angle i (degrees) and a bin width of 0.47 arcsec out to a radius, R''_{Ho}, corresponding to the position when the median surface brightness (uncorrected for inclination) in the ring is close to the Holmberg surface brightness, i.e. $\mu_B = 26.5$ mag arcsec^{-2}. The absolute magnitudes have been corrected for Galactic extinction according to Burstein & Heiles (1982). $\Delta\mu$ is the inclination correction of the surface brightness in magnitudes, $r_{\rm Mpc}$ is the distance in Mpc.

ESO id.	PA°	i°	$\Delta\mu$	R''_{Ho}	$r_{\rm Mpc}$	M_B	B	$B-V$	$V-R$	$V-I$	$V-J$	$J-H$	$H-K'$
338-04	162	61	0.79	42	38	−18.9	13.98	0.40	0.11	0.11	(0.85)[1]	(0.51)[1]	(0.25)[1]
338-04b[2]	135	58	0.69	-	38	-	-	-	-	0.58	1.58	0.57	0.04
350-38	120	35	0.22	24	82	−20.0	14.57	0.58	0.18	0.39	1.10	0.63	0.60
400-43	163	40	0.29	20	77	−19.6	14.89	0.62	0.00	-	0.48	0.63	0.23
400-43b[3]	40	70	1.16	26	77	−17.8	16.55	-	-	-	-	0.38	0.36
480-12	20	64	0.90	34	60	−18.9	14.96	0.37	0.13	0.44	1.00	0.70	0.14

1) The Holmberg radius could not be reached in the near-IR so the given colour is valid for a radius of 30 arcsec.
2) $m_V = 15.0$, $M_V = -18.3$ at $\Phi = 50''$.
3) $B-R = 0.40$, $B-J = 2.09$.

4. Results

4.1. Morphologies

In Figs. 2, 3 and 4 we present images and colour-index maps of the programme galaxies. The near-IR images are strongly limited by the small field size of the detector but in fact the profiles reach quite far out from the starburst region and it is hard to find corresponding data in the literature. In contrast to normal late type galaxies the BCGs show a strong morphological similarity between the optical and the near-IR. Since the visible light is dominated by young stars, the morphological similarity suggests that young stars (e.g. red supergiants) dominate the near-IR light as well. At intermediate light levels irregular structures, reminiscent of whisps, shells and tails show up. At fainter light levels a somewhat more regular structure is

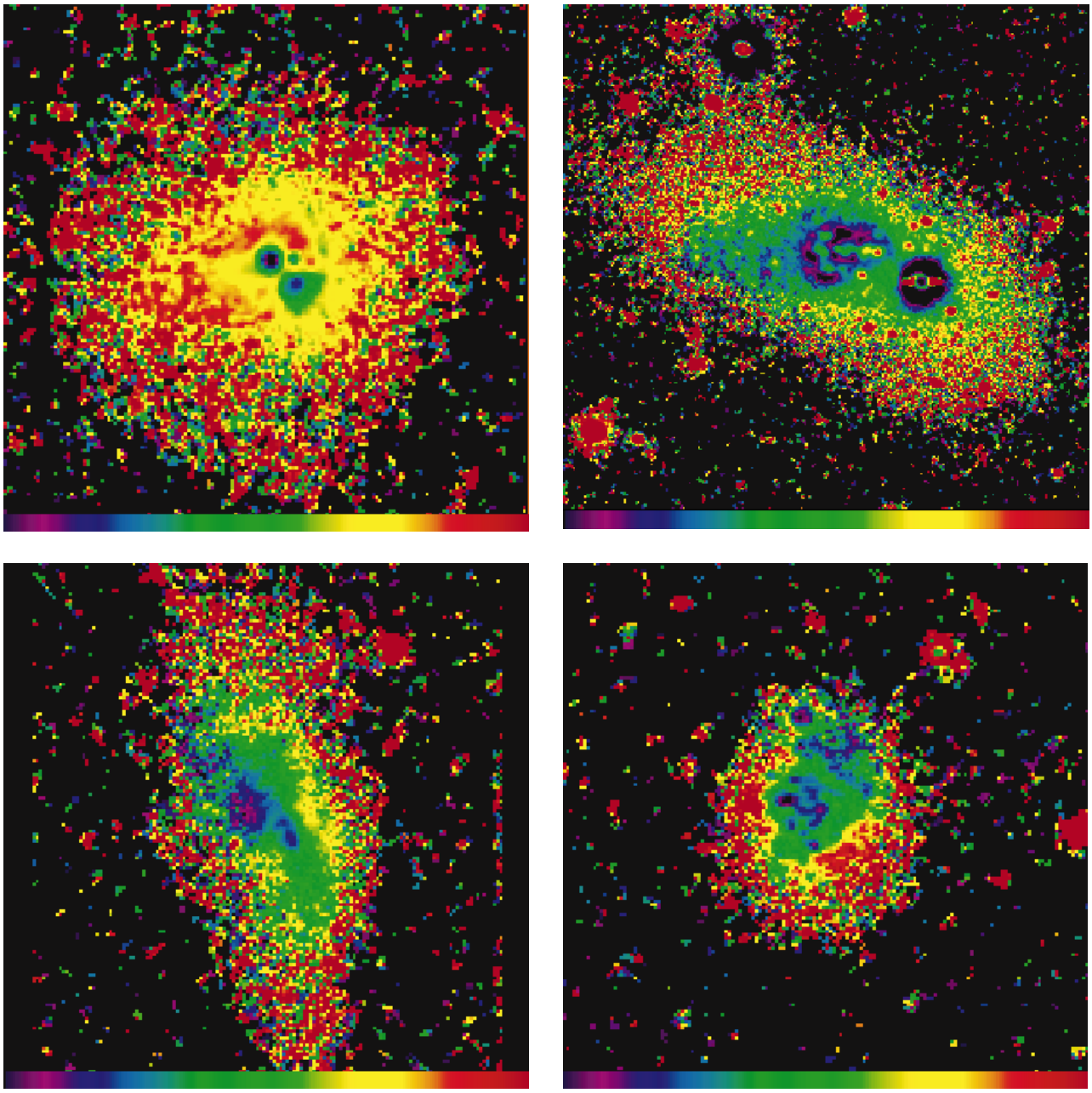

Fig. 4. $B - R$ colour-index maps of ESO 350-IG38 (upper left), 338-IG04 (upper right), 480-IG12 (lower left) and 400-G43 (lower right). The colour coding follows true colours with blue representing young star forming regions. The dynamical range has been chosen to enhance differences: for 350-38 and 338-04 the range is $B - R$ = 0.2–1.2, while for 480-12 and 400-43 it is $B - R$ = 0.2–1.0. North is up, east is to the left. The size of each image is $1' \times 1'$. The feature ∼15″ west of the centre in ESO 338-IG04 is a residual from the bright foreground star.

seen but at the faintest levels again we see no firm evidence of an equilibrium system.

4.2. General characteristics of the programme galaxies

Photometry and basic spectroscopic data of most of the galaxies were presented by Bergvall & Olofsson (1986). A study of the velocity fields in Hα of all the programme galaxies has been published (Östlin et al. 1999; Östlin et al. 2001).

4.2.1. ESO 338-IG04 (Tololo 1924-416)

This well-known BCG has been discussed by us in two previous papers (Bergvall et al. 1985; Östlin et al. 1998). The optical light is dominated by the central irregular starburst, clearly resolved into compact star clusters in HST images (Meurer et al. 1995; Östlin et al. 1998). At faint isophotal levels the morphology is that of a warped disk. In a filtered image (Fig. 6), where we have made an effort to enhance the faintest structures, a sharp edge-like structure is seen in the northeastern part of the

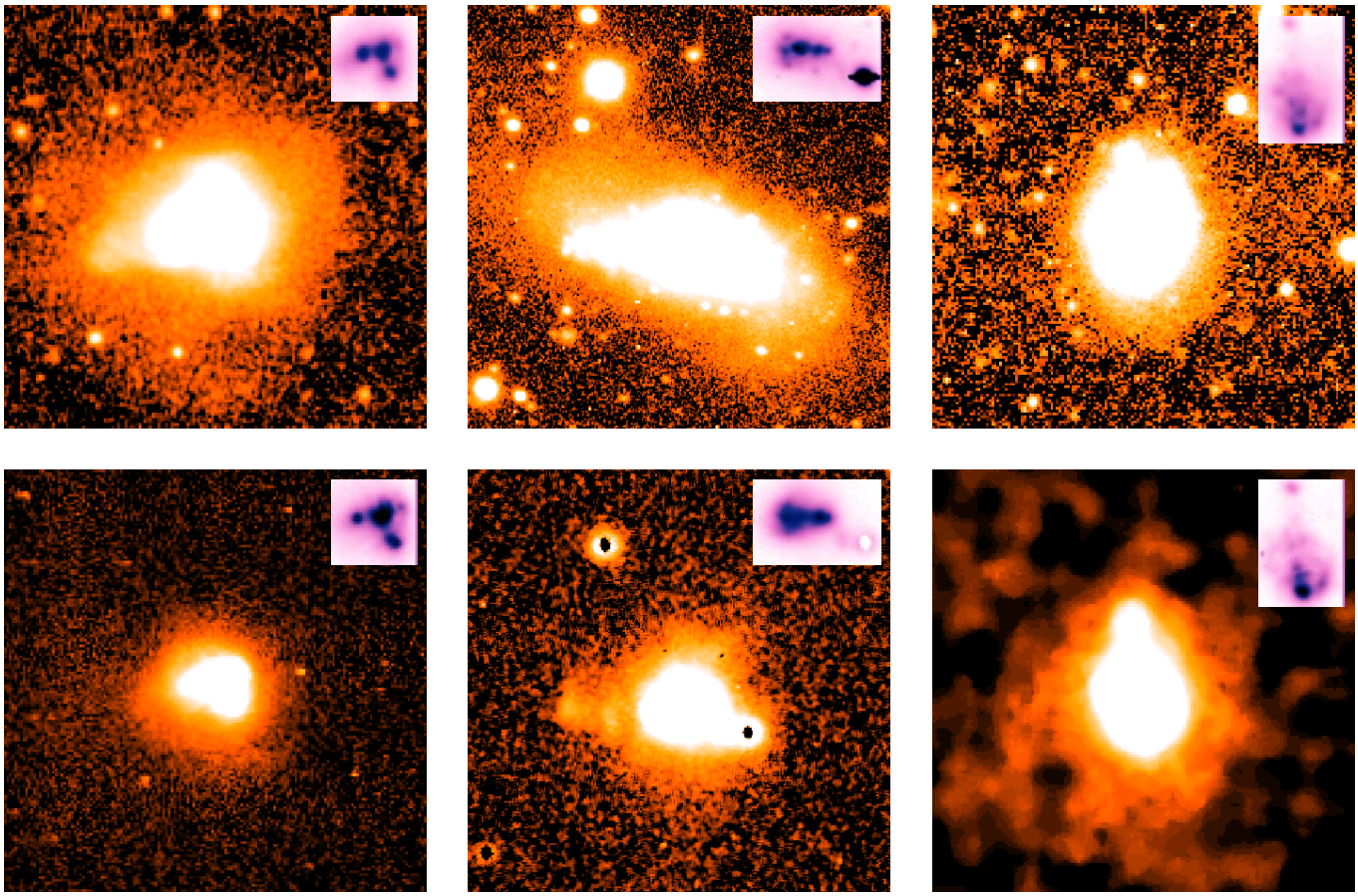

Fig. 5. The images shown are from left to right ESO 350-IG38, 338-IG04 and 400-G43. The upper panel shows deep images in the *R* window and the lower panel continuum subtracted Hα images. The inserts in the upper right corners are displayed to show the details of the central regions and have the same scale size as the larger images. The field size is $1.2' \times 1.2'$. North is up, east is to the left. (ESO 1.5 m D, MPG/ESO 2.2 m and NTT telescopes.)

disk, possibly indicating a warp or a shell. Hα kinematics derived from the Fabry-Perot spectroscopy (Östlin et al. 2001) reveal what may be interpreted as two dynamically separate systems, as if the galaxy went through a merger. Figure 4 shows a clear distinction in colour between the starburst and the surrounding host galaxy. Moreover, there is a blue tail, with peculiar kinematics (Östlin et al. 2001) extending eastwards from the starburst. In the Hα image (Fig. 5, see also Fig. 7) we see structures extending perpendicular to the plane, probably due to nebular emission from bipolar outflows.

This galaxy is of particular interest because it has been shown to host a system of globular clusters, found to have a range of ages, from young ones to old (Östlin et al. 1998). The distribution in age indicates that the galaxy has had a few active starburst periods in the past. The maximum duration of the current burst is estimated from the HST data to be less than 100 Myr or more probable 50 Myr, and the last previous major burst probably occurred about 2 Gyr ago. The centre of the distribution of the globular clusters is offset with respect to the starburst but agrees with that of the underlying red component.

Bergvall (1985) reported an increase in the optical brightness between 1979 and 1983 and Gondhalekhar (1986) reported an increase in the UV brightness during the same period. Our new data from 1997 and recent data from Doublier (1999) seem to confirm that the galaxy is variable in the optical. A comparison between our near-IR photometry from different epochs shows no variability. Bergvall & Olofsson (1986) obtained with a diaphragm of 15 arcsec $J = 13.3 \pm 0.1$, $H = 12.7 \pm 0.1$, $K = 12.5 \pm 0.1$ as compared to 13.2 ± 0.04, 12.7 ± 0.04 and 12.4 ± 0.05 from our integrated surface photometry of the IRAC2 images in a circular aperture. Variability in the galaxy will seriously affect the interpretation of the photometry of the central region discussed below but should not affect the halo data.

4.2.2. ESO 338-IG04b

This is a spectroscopically confirmed companion of the former galaxy (Bergvall unpublished; see also Östlin et al. 1999). Morphologically it could be classified as a late type dwarf irregular, with moderate star formation activity. Contrary to ESO 338-IG04 it shows regular kinematics, and a dynamical mass model shows that it contains dark matter (Östlin et al. 1999, 2001). It may have a smaller companion ~40″westwards (see Fig. 2).

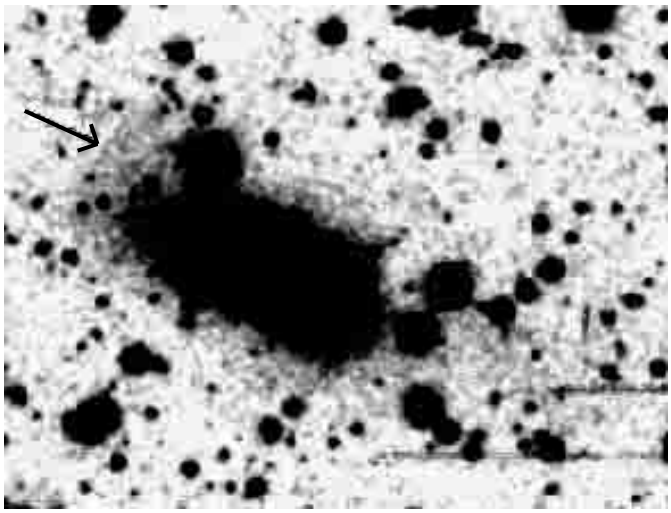

Fig. 6. A deep, median-filtered image of ESO 338-IG04 in V. The arrow on the left side indicates what might be a remnant of a disk participating in a merger. The field size is $2.9' \times 2.2'$. North is up, east is to the left. ESO NTT.

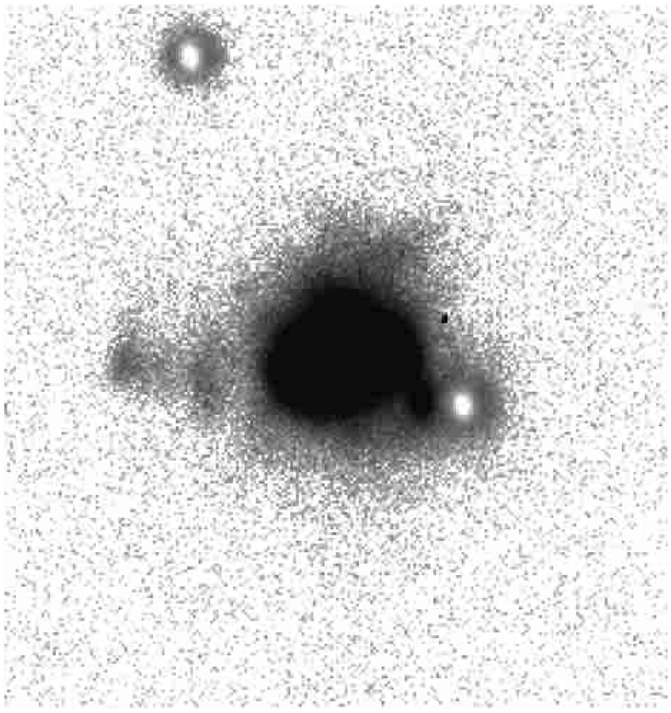

Fig. 7. A map of the equivalent width of Hα in emission of ESO 338-IG04. The continuum subtraction was made using a Hα filter tuned at a different redshift. The displayed range in $W_{\mathrm{H}\alpha}$ is ~0–500 Å and the darker parts correspond to the largest values. The values in the halo are ≤10 Å. The two blobs with bright centers are residuals from bright stars. The field size is $1.1' \times 1.1'$. ESO NTT.

4.2.3. ESO 350-IG38 (Haro 11)

Three bright condensations are seen in the centre of the galaxy, which hosts a strong starburst as evident from the high excitation, large emission line equivalent widths and a strong signature of emission lines from WR stars in the spectral region around HeII λ4686. Haro 11 is also an extremely hot IRAS source (Bergvall et al. 2000). While the broadband images show three condensations in the centre, Fig. 4 shows two blue hotspots. However, the $W_{\mathrm{H}\alpha}$ image (Fig. 8) shows that the third condensation has the highest $W_{\mathrm{H}\alpha}$ value. The colourmap shows a gradual transition to redder colours with distance from centre. The central bent structure can be followed to faint isophotal levels, which together with the peculiar kinematics, strongly suggest a merger origin of the starburst (Östlin et al. 2001).

Östlin (2000) revealed the presence of a large number of globular cluster candidates, similar to the ones in ESO 338-IG04. Faint whisps and indications of shell structures are seen in the faint outskirts of the mainbody. Approximately perpendicular to the apparent major axis (which has a position angle ~110°), the Hα distribution is extended, suggesting the presence of bipolar outflows of ionised gas (Fig. 5). Also $W_{\mathrm{H}\alpha}$ is enhanced south of the centre, in approximately the same direction (Fig. 8).

We observed this galaxy in HI with the VLA, the Nancay antenna and with the Parkes antenna (all unpublished) but only an upper limit of the HI mass of $\mathcal{M}_{\mathrm{HI}} < 10^8\ \mathcal{M}_\odot$ could be obtained. With a $\mathcal{M}_{\mathrm{HI}}/\mathcal{M}_{\mathrm{tot}} < 0.01$, this galaxy seems to be remarkably devoid of neutral hydrogen. We made an effort to quantify the conditions in Haro 11 on basis of observations carried out in the far-IR using the ISO LWS (Bergvall et al. 2000). We concluded that most of the neutral HI was located in photodissociated regions. Starting from the simplified situation discussed in Sect. 5 we may derive an estimate of the mass of the ionised hydrogen gas. From the spectroscopy we calculate a central electron temperature of $T_{\mathrm{e}} = 13\,700 \pm 300$ K and density of $n_{\mathrm{e}} \sim 10$ cm^{-3}. The Hα luminosity is 3.2×10^{35} W. From this number we derive a mass of the ionised gas inside 2 scalelengths of $10 \pm 1 \times 10^8\ \mathcal{M}_\odot$, assuming a filling factor of 0.01–0.1. The mean HI mass of BCGs of the size of Haro11 is $8.1 \pm 0.2 \times 10^8\ \mathcal{M}_\odot$ (Gordon & Gottesman 1981). In Bergvall et al (2000) we estimate the fraction of molecular gas and the mass of the gas in the photodissociated regions to be $\geq 3 \times 10^8\ \mathcal{M}_\odot$. These numbers show that a major fraction of the gas may be in ionised and molecular form.

4.2.4. ESO 400-G43

As Fig. 4 shows, this galaxy has a blue irregular, clumpy central region and a red regular halo. 2 arcmin east of ESO 400-G43 is a companion galaxy, here named ESO 400-G43b, detected from the HI observations of the main component (Bergvall & Jörsäter 1988). Jörsäter & Bergvall (unpublished) observed the main component at the VLA in the 1415, 4885 and 8414 MHz windows. While the continuum slope in the low frequency range agrees with that of Bremsstrahlung radiation from the ionised gas, a component with a steep spectral index $\alpha \sim -1.2$ ($S^\nu \propto \nu^\alpha$) shows up near the centre. Possible sources are radiosupernovae, SN remnants or possibly a low-mass AGN. Figure 5 shows a median filtered Hα image of the galaxy. The galaxy has a very extended Hα halo that can be followed out to 4–5 kpc, or ~2 scalelengths. The $W_{\mathrm{H}\alpha}$ map is shown in Fig. 9. A longslit spectrum across the galaxy indicates that the extinction is close to zero throughout the central region (Fig. 11).

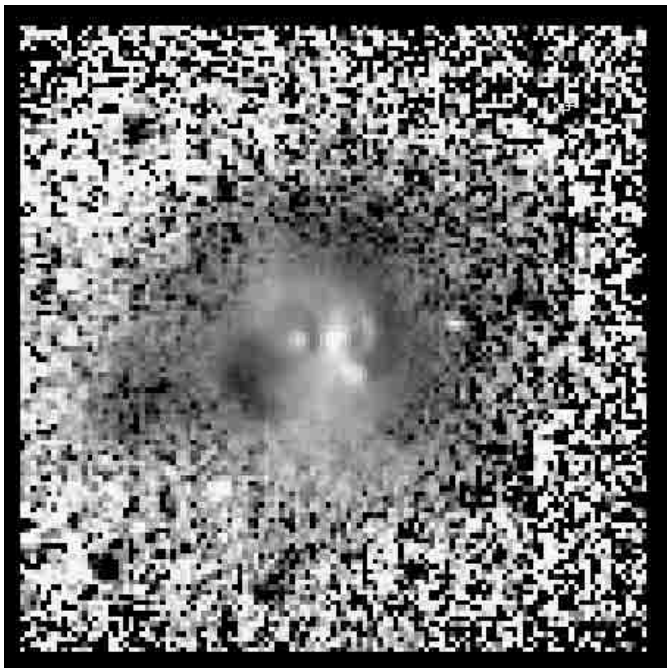

Fig. 8. A map of the equivalent width of Hα in emission of ESO 350-IG38. The range in $W_{\mathrm{H}\alpha}$ is 0–700 Å and the brighter parts correspond to the largest values. The values in the halo are about 50 Å except in the southernmost direction where it reaches a few hundred. The field size is $1' \times 1'$. ESO 1.5 m Danish telescope.

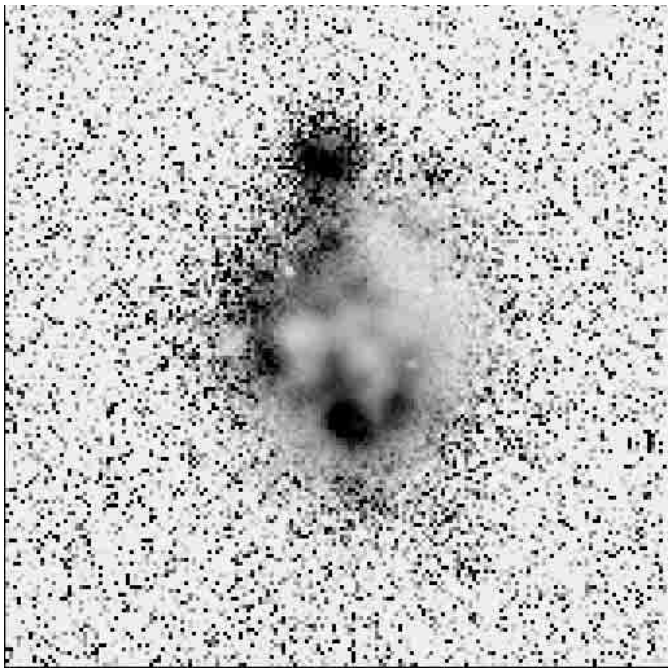

Fig. 9. A map of the equivalent width of Hα in emission of ESO 400-G43. The continuum subtraction was made using a Hα filter tuned at a different redshift. The displayed range in $W_{\mathrm{H}\alpha}$ is ~0–500 Å and the darker parts correspond to the largest values. ESO NTT.

The dynamics and HI content of this galaxy were discussed by Bergvall & Jörsäter (1988). One of the purposes with that investigation was to use dynamical information to set upper limits to the mass of older stellar generations. This mass determination is particularly important since it is derived from an HI rotation curve reaching far outside the optical extent of the galaxy and as such is unique in our sample. The HI mass is $\sim 5 \times 10^9$ $\mathcal{M}_\odot$ and for the companion 4×10^9 $\mathcal{M}_\odot$. A smaller cloud with a mass of approximately 1×10^9 $\mathcal{M}_\odot$ and no optical counterpart was detected NW of the main component, suggesting that we may be witness to a merging of a smaller group of galaxies and gas clouds. From best fits to the rotation curve of the optically bright central region it was found that the mass was $\sim 1.3 \times 10^9$ $\mathcal{M}_\odot$, close to the photometric mass estimate of young stars and ionised gas. Moreover, when corrected for internal extinction (using the Hα/Hβ ratio) the colours ($U - B \sim -0.8$; $B - V \sim 0.1$) correspond to a young stellar population. These observations led Bergvall and Jörsäter to suggest that ESO 400-G43 could be a galaxy still in the state of formation. They also showed that dark matter dominates the dynamics at $r > 15$ kpc and that the total mass was $>10^{10}$ $\mathcal{M}_\odot$, if dynamical equilibrium was assumed. A distorsion in the transition between the stellar disk and the HI was interpreted as either an effect of gas infall or a warp. Östlin et al. (1999, 2001) mapped the central kinematics in Hα and confirmed the complexity of the velocity field in the nort-eastern part of the central disk, making dynamical mass determinations of the centre more uncertain.

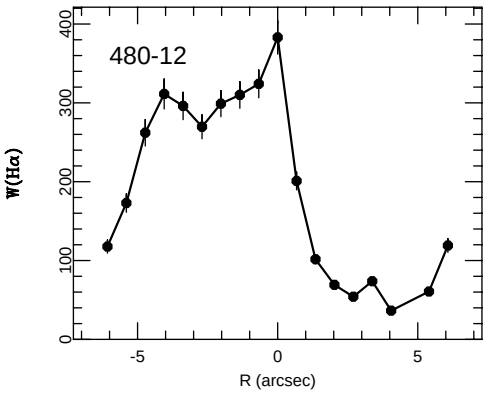

Fig. 10. $W_{\mathrm{H}\alpha}$ as derived from a slitspectrum across the central region of ESO 480-IG20 in a position angle of 20°. The error bars are estimated 1 σ mean errors.

4.2.5. ESO 400-G43b

This is the companion of the previously discussed galaxy. It has properties of an extensively ionised dI galaxy embedded in an HI cloud with mass 4×10^9 $\mathcal{M}_\odot$, and a $\mathcal{M}/L$ ratio that is normal for dIs. Both the spatial extent and equivalenth width of the Hα emission are considerably smaller than for the main component. The excitation, as measured from the [OIII]λ5507/Hβ ratio is moderate, and the galaxy is not a strong IRAS source. Hence, this is not a starburst galaxy.

4.2.6. ESO 480-IG12

This galaxy has a central condensation and a morphology at the fainter levels that resemble a warped, distorted disk. It is

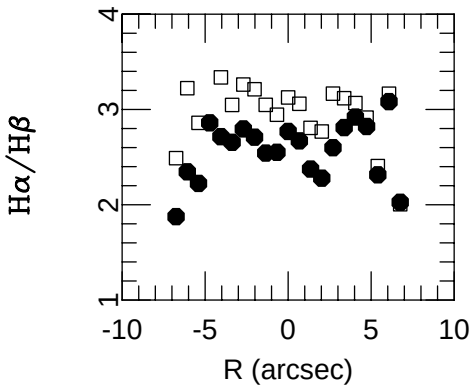

Fig. 11. The Hα/Hβ emission line ratio as derived from a slitspectrum across the central region of ESO 400-G43. The open squares are the observed data and the filled circles are the data after corrections for underlying absorption in the Balmer lines.

the brightest component in a chain of galaxies (see Östlin et al. 2001, Fig. 7). We obtained spectra of three of these (unpublished). They all have high velocities and thus probably do not belong to the system. The colour index map (Fig. 4) shows a blue spiral-like structure slightly off centre. ESO 480-IG12 has the lowest $W_{\mathrm{H}\alpha}$ of the BCGs studied (buth higher than the two companions). Irregular, warp-like structures are seen in the outer isophotes. Also in this galaxy very faint structures stretch out in a direction perpendicular to the disk, indicating that we have bipolar outflows of gas. Further support for this comes from our Fabry-Perot spectroscopy (Östlin et al. 1999, 2001).

4.3. Internal extinction

Comparisons between observations of star forming galaxies and predictions from SEMs are strongly dependent on the reliability of the extinction corrections. In massive star forming galaxies this may become a very severe problem since we may have a radial dependence on metallicity, age and extinction that results in a degeneracy in the information obtained, if the wavelength region covered is not sufficiently extended. The situation is more favourable in studies of BCG as most observations of BCGs point at a low dust content, even in the very central regions (e.g. Terlevich et al. 1991). This is confirmed also for the objects discussed in this article as will be shown below.

Since we, at this step, are primarily interested in obtaining information about the halo population, the first thing is to secure that 1) the extinction is low and 2) the contribution from nebular emission can be controlled. We will use slit spectra to determine the extinction from the Hα/Hβ ratio. Since the Balmer emission lines are affected by the Balmer absorption lines from the young stellar population, they have to be corrected for this before they can be used for extinction measurements. As a first approximation, the correction was based on $W_{\mathrm{H}\alpha}$ in comparison with predictions from our SEMs. In Fig. 11 we show the results from a slitspectrum of one of the programme galaxies, ESO 400-G43. We show both the measured Hα/Hβ ratio and the same ratio after correcting for underlying absorption based on $W_{\mathrm{H}\alpha}$. From the diagram we see that the corrected Hα/Hβ ratio several times falls significantly below the theoretical ratio based on Brocklehursts data (Brocklehurst 1971) which we approximately express

$$F(\mathrm{H}\alpha)/F(\mathrm{H}\beta) = 4.825 - 0.478 \cdot \log\,(T_{\mathrm{e}}). \quad (1)$$

What is the reason for this deviation? When comparing with slit spectra from other observing runs, covering the same region of the galaxy, we can convince ourselves that there are no problems with the calibration. The problem is probably due to what seems to be an erroneous correction for underlying absorption. It seems that the correction should be smaller than what we have used. The most likely explanation is that we have encountered the problem discussed above, i.e. that we underestimate $W_{\mathrm{H}\alpha}$ either because of leakage along optically thin paths from the centre and outwards, or because much of the light from the HII region actually falls outside the slit. The second explanation seems to be most probable. A more realistic correction is to use the colours of the starburst to select a best-fit SEM, after iteratively correcting for underlying absorption based on the Hα/Hβ ratio. From this model we then obtain the equivalent widths we need. These turn out to be intermediate between the no correction and the correction based on $W_{\mathrm{H}\alpha}$. We will use this method to determine the chemical abundances as discussed below. The conclusion as regards the extinction in the case we discussed above is that it is low ($E(B-V) < 0.1$ mag) and shows little variation across the galaxy. We cannot say for certain that it does not increase in the halo but we see no indications of this in the two colour images. We will therefore assume that the light from the halo is fairly unreddened. That is, when we derive the parameters of the luminosity profiles we will make a simple correction for internal reddening, assuming that the optical depth is proportional to the disk thickness where the zeropoint is taken from the derivation of the extinction from the central region. The corrections will be quite small however.

4.4. Chemical abundances

The chemical abundances of nitrogen and oxygen of all galaxies except ESO 338-IG04 were derived both from IDS spectra and EFOSC1 spectra. For ESO 338-IG04 Bergvall (1985) derived 12 + log(O/H) = 8.07, whereas Masegosa et al. (1994) and Raimann et al. (2000) both got 12 + log(O/H) = 7.92.

The intensities of the most prominent emission lines relative to Hβ of the remaining three BCGs and the two companions are presented in Table 4. For the brighter central regions of the galaxies the calculation of the emissivity of the O^{++} zone was based on a determination of the electron temperature from the [OIII]λ4363/[OIII]$\lambda\lambda$4959, 5007 emission-line ratio. From the first calculation of T_{e} we derived the theoretical Hα/Hβ recombination value (Brocklehurst 1971) We then made a reddening correction according to above and derived a new T_{e}. In this way the extinction and the temperature in the O^{++} region were iteratively determined. In order to calculate the total oxygen abundance one would like to know also the temperature of the O^{+} zone. Since useful lines for such a calculation are either too weak or outside the spectral window we calculate this temperature from the metallicity dependent relations derived by Vila-Costas & Edmunds (1993) on basis of

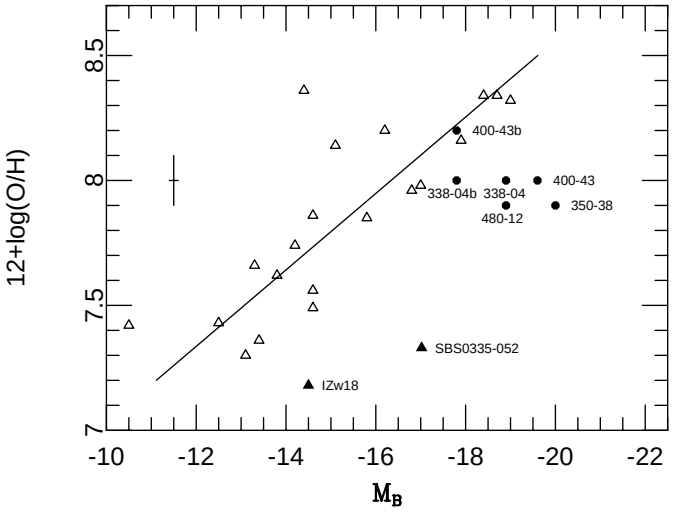

Fig. 12. The oxygen abundance of the target galaxies as function of absolute blue magnitude. The open triangles are local group dwarf galaxies and the full drawn line is the regression line. Data are from Skillman (1989). Also shown are the positions of two young galaxy candidates, IZw18 and SBS0335-052.

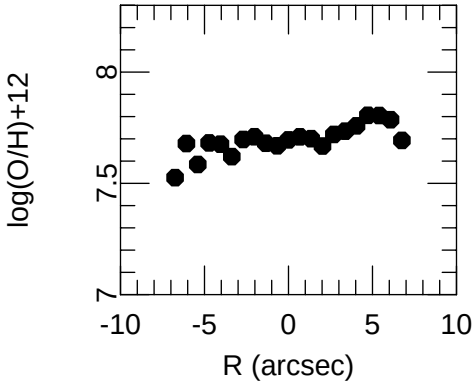

Fig. 13. The oxygen abundance of ESO 400-G43 as a function of position along the disk. The position angle is 110 degrees. The abundances are derived from McGaugh's empirical relations (McGaugh 1991, 1994), utilizing the [OII], [OIII] and Hβ lines.

Stasińskas (1990) models. If T_e is expressed in units ot 10^4 K, the equation we use in this case is

$$(T_e(O^+))^{-1} = 0.55(T_e(O^{++}))^{-1} + 0.36. \quad (2)$$

The total oxygen abundance was then calculated from the [OII]λ3727 and [OIII]λ4959, 5007 lines using atomic constants from Mendoza (1983). The derived abundances are all ∼10% solar for the BCGs and slightly larger for the companions. In Fig. 12 we compare the metallicities with the metallicity-luminosity relationship derived for the local group galaxies (Skillman 1989). We note that the 4 luminous BCGs, but not the companions, deviate significantly from the relationship. The deviation of our most extreme cases from the Skillman et al. line is the same as for the two young galaxy candidates, IZw18 and SBS 0335-052.

A useful piece of information in the interpretation of the difference in metallicity between the populations in the different regions of the galaxies is the size of possible abundance gradients in the ionised gas across the centre and out into the halo. To check the homogeneity of the oxygen abundances over the starburst regions we have to work at faint levels in the spectra, where the standard method cannot be used. For this purpose we applied the empirical relations based on the ([OII]λ3727+[OIII]$\lambda\lambda$4959,5007)/Hβ line ratio (Pagel et al. 1979; Pagel et al. 1980; Edmunds & Pagel 1984; Skillman 1989). We are not concerned in this article with systematic differences between the abundances derived from the temperature sensitive method and the empirical method since we only wish to set limits on the amplitude of the fluctuations in the abundances. As an example the result from ESO 400-G43 is shown in Fig. 13. We see that the variations in the abundances are quite small, and within the accuracy of the empirical method. The central oxygen abundances are presented in Table 4 along with the nitrogen abundances as derived from the [NII]λ6584 line and the assumption N/H = $(N^+/H^+)/(O/O^+)$.

4.5. Luminosity and colour profiles

Figures 14 to 16 show the optical/near-IR luminosity and colour profiles of the galaxies. We wish to point out that the on-the-spot colours within the central 1–2 arcsec are not reliable due to seeing effects. To simplify the presentation we will only show the B luminosity profile (except for ESO 338-IG04 where we also show the V profile reaching a photometric level of unique depth) and a few colour index profiles. This will be sufficient for our main goal here which is to separate the halo population from the young burst. Of course there may be many different components in the galaxy if several mergers have occurred but we will show below that it really is possible to use a two component distinction. Many investigations of the stellar population in BCGs are based on BVR surface photometry. A problem when using only BVR data is that the colour indices, in particular $B-V$, are fairly insensitive to age if the metallicity is low. It is thus difficult to use these colours to discriminate between the burst population and an old halo population. Moreover the old generation has difficulties to compete with the luminous young generation. Therefore a combination of optical and near-IR colours is much more powerful, as is evident the diagrams. In particular in the $V-K'$ profile which is shown in the diagram, we see a strong trend towards redder colours as we move outwards. Although this trend is present also in the $B-V$ colours it is much weaker, despite that we have corrected the colours we show in the diagrams for internal extinction. This is due to the compensating effect nebular emission has on "age reddening". We will call the red stellar population the "halo population", clearly distinguished from the starburst population in the centre.

What we now will do is make a fit to this part of the luminosity profiles of the deepest images to see what restrictions we can set to the shape of the profile. In general (e.g. Sersic 1968;

Table 4. Emission line fluxes and derived properties of the nebular gas. The top line gives the ESO numbers of the target galaxies and the second line the aperture that the fluxes are referred to, centered on the brightest part of the galaxy in the visual region. Line fluxes are relative to Hβ. F is the measured emission line flux relative to Hβ and F_c is the extinction corrected emission line flux relative to the Hβ line flux corrected for underlying absorption. n_e is the electron density derived from the [SII] lines. Typical errors in the fluxes are 5% for the strong lines and 10% for the weaker ones. Oxygen and nitrogen abundances are in log units. The mean errors in the abundances are typically 0.1–0.2 dex.

Line id.	338-04b		350-38		400-43		400-43b		480-12	
	2″ × 2″		4″ × 4″		2″ × 0.7″		4″ × 2″		4″ × 4″	
	F	F_c	F	F_c	F	F_c	F	F_c	F	F_c
[OII] λ3727	1.73	1.74	1.76	2.02	4.68	4.39	4.82	3.98	2.40	2.54
[NeIII] λ3869	0.30	0.30	0.18	0.20	-	-	-	-	0.36	0.37
[OIII] λ4363	0.033	0.030	0.050	0.051	0.058	0.054	-	-	0.067	0.064
HeI λ4471	0.059	0.053	0.039	0.039	-	-	-	-	0.043	0.041
[OIII] λ4959	1.25	1.02	1.19	1.05	1.14	1.05	1.00	0.83	1.46	1.22
[OIII] λ5007	3.69	3.00	3.80	3.30	3.32	3.06	3.24	2.68	4.64	3.86
HeI λ5875	0.16	0.11	0.15	0.11	0.17	0.15	-	-	0.14	0.10
[OI] λ6300	0.16	0.11	0.068	0.047	0.20	0.18	-	-	0.073	0.050
Hα	4.13	2.76	4.08	2.75	3.12	2.82	3.42	2.82	4.12	2.75
[NII] λ6584	0.13	0.08	0.78	0.52	0.13	0.12	0.17	0.14	0.33	0.22
HeI λ6678	-	-	0.0268	0.018	-	-	-	-	-	-
[SII] λ6716	0.54	0.36	0.25	0.16	0.39	0.36	-	-	0.26	0.17
[SII] λ6730	0.44	0.30	0.13	0.086	0.25	0.22	-	-	0.19	0.12
$T_{e,[OIII]}$		11600		13700		14400		-		14100
log $n_{e,[OIII]}$		2.3		0.8		0.8		-		1.8
$T_{e,[OII]}$		12000		13100		13400		-		13200
log $n_{e,[OII]}$		2.3		-0.2		-0.2		-		1.8
log(O/H) + 12		8.0		7.9		8.0		8.2[1]		7.9
log(N/O)		-1.5		-0.7		-1.7		-1.7		-1.2
$W_{H\beta}$ (Å)	32	38	65	72	32	38	15	18	43	51
$F_{H\beta}$ (10^{-18} $W m^{-2}$)	5.3	12.6	416	1120	39	46	4.5	5.4	167	366

1) Based on the empirical oxygen abundance relationship by McGaugh (1991).

Graham et al. 1996), the luminosity profiles of galaxies may be expressed as

$$I(r) = I_e \exp\left(-b[(\frac{r}{r_e})^{1/n} - 1]\right) \quad (3)$$

where r_e is the effective radius, enclosing half of the light of the galaxy and b and n are constants. This relationship may also be expressed as

$$\mu(r) = \mu_0 + \frac{2.5b}{\ln(10)}\left(r/r_e\right)^{1/n} \quad (4)$$

where μ_0 is the central surface brightness. The constant b is a function of n and can be expressed as $b_n \approx 2n - 0.327$ (Capaccioli 1989). $n = 4$ for a de Vaucouleurs profile and $n = l$ for an exponential profile. The first shape is characteristic of normal ellipticals and the second one is typical of disks and dEs. Luminous cluster ellipticals have $n \leq 15$. There seems to be a continuous transition between the two extremes that occurs when going from high luminosity Es to low luminosity dEs (Graham et al. 1996).

4.6. Structural parameters

In an effort to disentangle the photometric parameters of host galaxies of BCGs, Papaderos et al. (1996) used luminosity profiles obtained from optical broadband images. When fitting an exponential disk to the outer part of the profile they found that the central surface brightness of this hypothetical disk was brighter than that of typical LSBGs ($\mu_{B,0} \geq 23$). The conclusion was that LSBGs were rather improbable as precursors of BCGs. In the present investigation we reach fainter limiting isophotes than they obtained in their work. Our luminosity profiles show that this may make a big difference. We see that the scalelength is more or less continuously increasing when going to lower surface luminosity levels. The faintest luminosity profiles of our galaxies reach ~29–30 mag arcsec^{-2} (n.b.: after correction for inclination). As shown in the figures, we get completely different results if we make a fit out to this isophote than if we stop at the more commonly used limit, $\mu_B \sim 25$–26 mag arcsec^{-2}. In fact we have no problem to reach a central

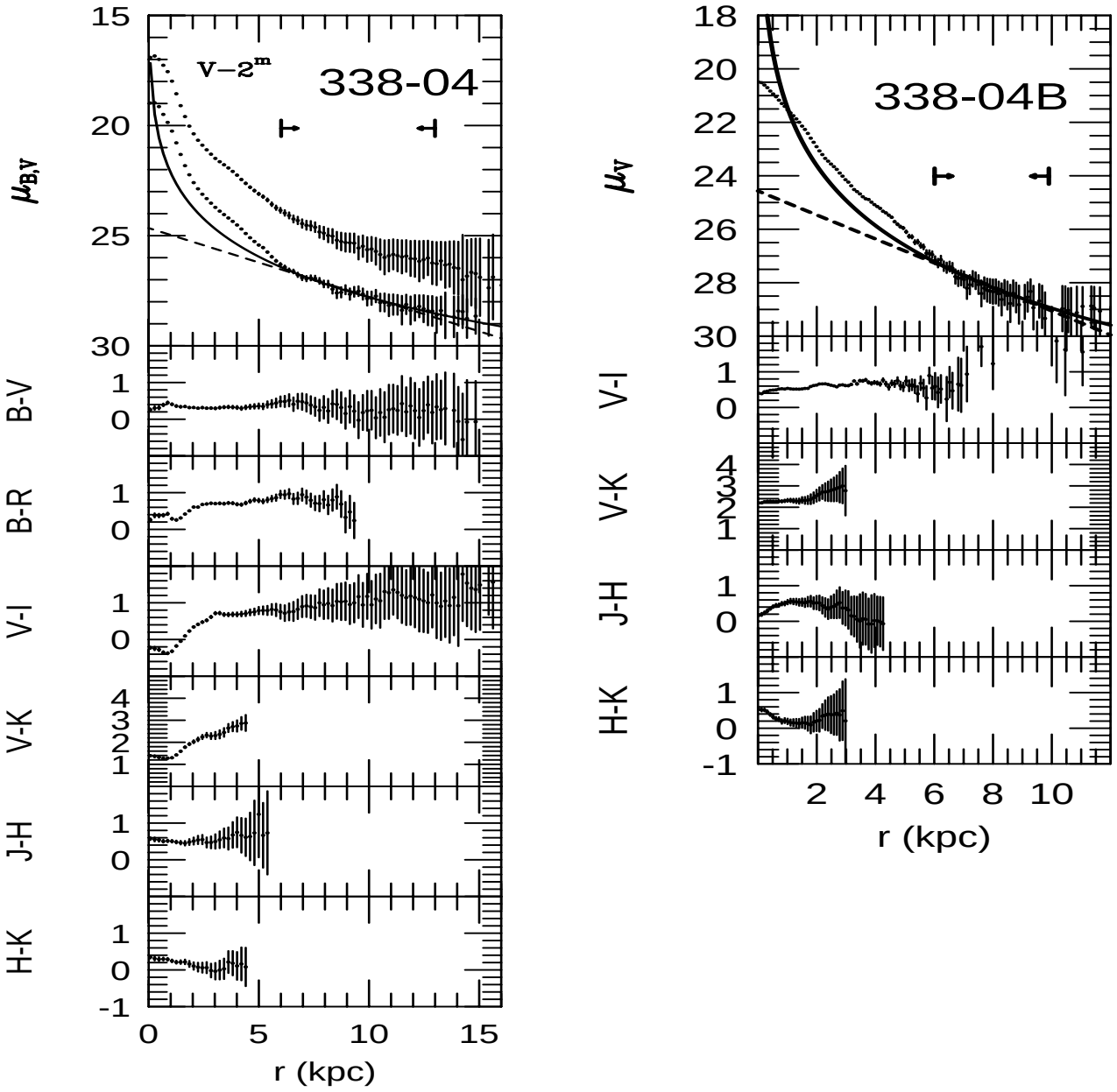

Fig. 14. The surface luminosity profiles of ESO 338-IG04 and ESO 338-IG04b in Cousins B and in Cousins/Johnson broadband colour indices. The luminosity profiles are shown with two different fits. The dashed line shows a least square fit to an exponential profile and the solid line a fit to a Sersic law. Inclination corrections based on a fit to the outer isophotes have been applied. Likewise reddening corrections based on spectroscopy of the central region and assuming the column density of the dust to be proportional to the luminosity density in the broadband image used to derive the upper luminosity profile, have also been applied. The error bars are 1σ deviations including the most pessimistic estimate of the error in the zero-point correction of the sky background.

surface brightness as low as that of LSBGs by fitting an exponential profile to the outer isophotes. The question is however, whether a disk really is the best and most appropriate fit.

To proceed we will make two fits to the outer isophotes, one where we leave the parameter n (Eq. (4)) free and one where we fix it to $n = 1$ (exponential disks), in order to facilitate comparisons with LSBGs. The range of the fit is set by eye inspection where the halo colours start to become significant. In Table 5 we summarize the parameters we derive from fits to the outer parts of the luminosity profiles, within the radial ranges as indicated as in the figures. The parameters we specify are the same as in Eq. (4). What is striking is that the n parameter is very large ($\gg$4) when we use good data at large distances from the centre. Although the baseline of the fit is short, which will make the solution somewhat unstable, we take this as an indication that the host galaxy of the burst is of early type since all galaxies go in the same direction. The fit will not be much worse if we fix n to be equal to 4 but we see no reason why we should prefer this value to the best solution value. We obtain an even better fit (measured by the correlation coefficient) to a power-law if we include more data points closer to the centre. In the final column of the table we give the maximum luminosity

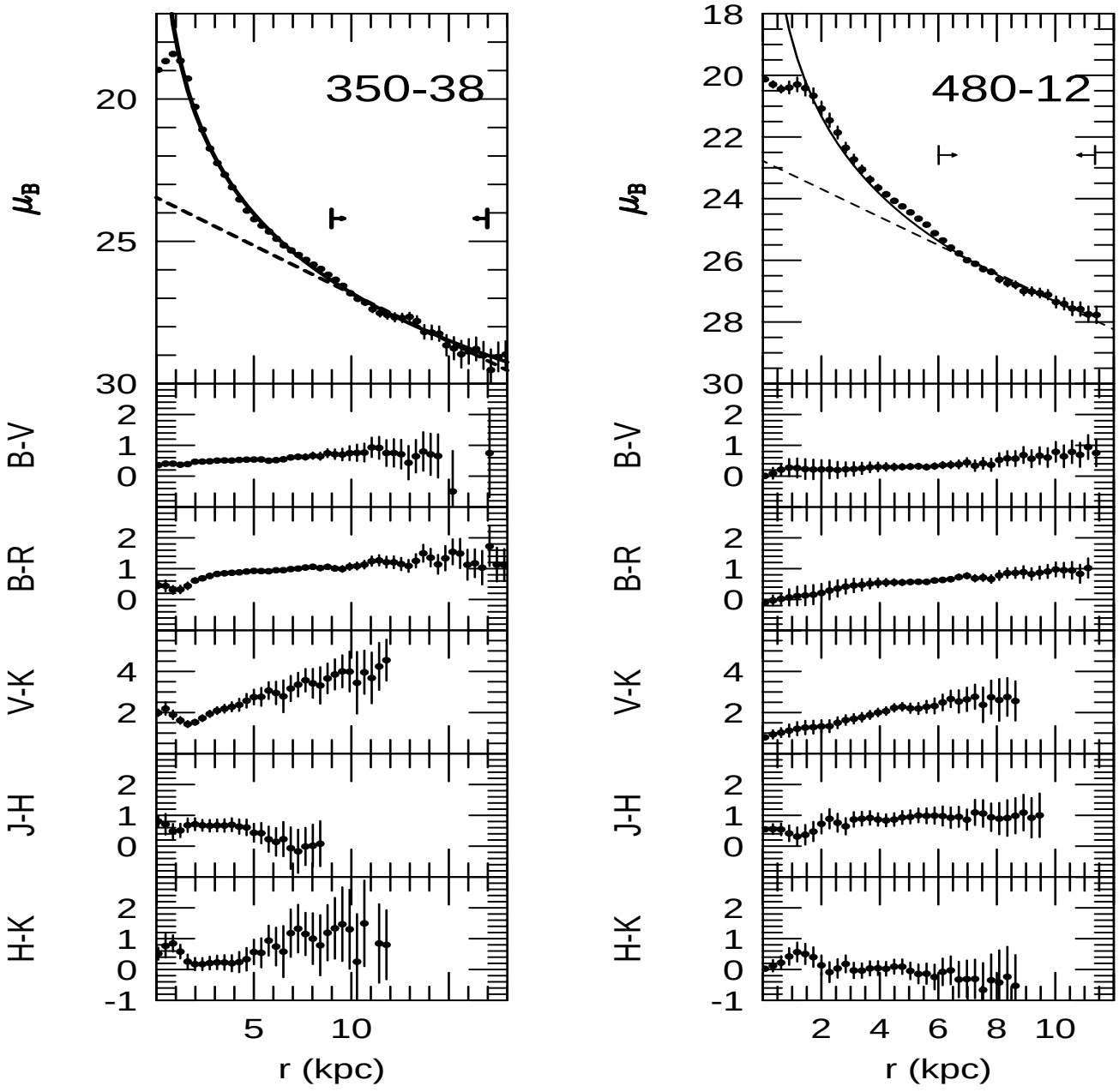

Fig. 15. Luminosity and colour index profiles of ESO 350-IG38 (Haro 11) and ESO 480-IG12.

the power law component can have, simply by assuming that the brightness follows the power law down to a distance where the model surface brightness is equal to the observed surface brightness. At shorter radial distances we have assumed it to be equal to this value.

There is an exciting consequence of the high n values we derive, should these values turn out to be firm, once deeper photometry becomes available. Caon et al. (1993) found a correlation between n and galaxy luminosity. The higher the n value the brighter (and more massive) the galaxy. Similarly, Graham et al. (1996) found that bright cluster ellipticals typically have high n values. The highest best fit n values for the luminous galaxies is typically $n \sim 15$. If a high n signals a high mass it could indicate that the BCGs in our sample have a high amount of dark matter.

5. Nebular emission from the halo region of BCCs

In a few cases optical colours of the halos of BCGs have been derived that have been taken as evidence of an old stellar population (Hunter & Gallagher 1985; Kunth et al. 1988). However, one has to be aware of the ambiguities in the interpretation of these data. The analysis of our programme galaxies shows that nebular emission may contribute with a considerable amount to the light from the halo. Possible in situ ionising sources are young stars or old hot stars, i.e. blue horizontal branch stars (BHB) or post-AGB stars (PAGB). If so, it would cause no problem in the following comparisons with SEMs predictions, since the ionising flux from these stars is taken into account and the nebular component is included in the models. But, as we will show below, it is quite possible that gas in the halo

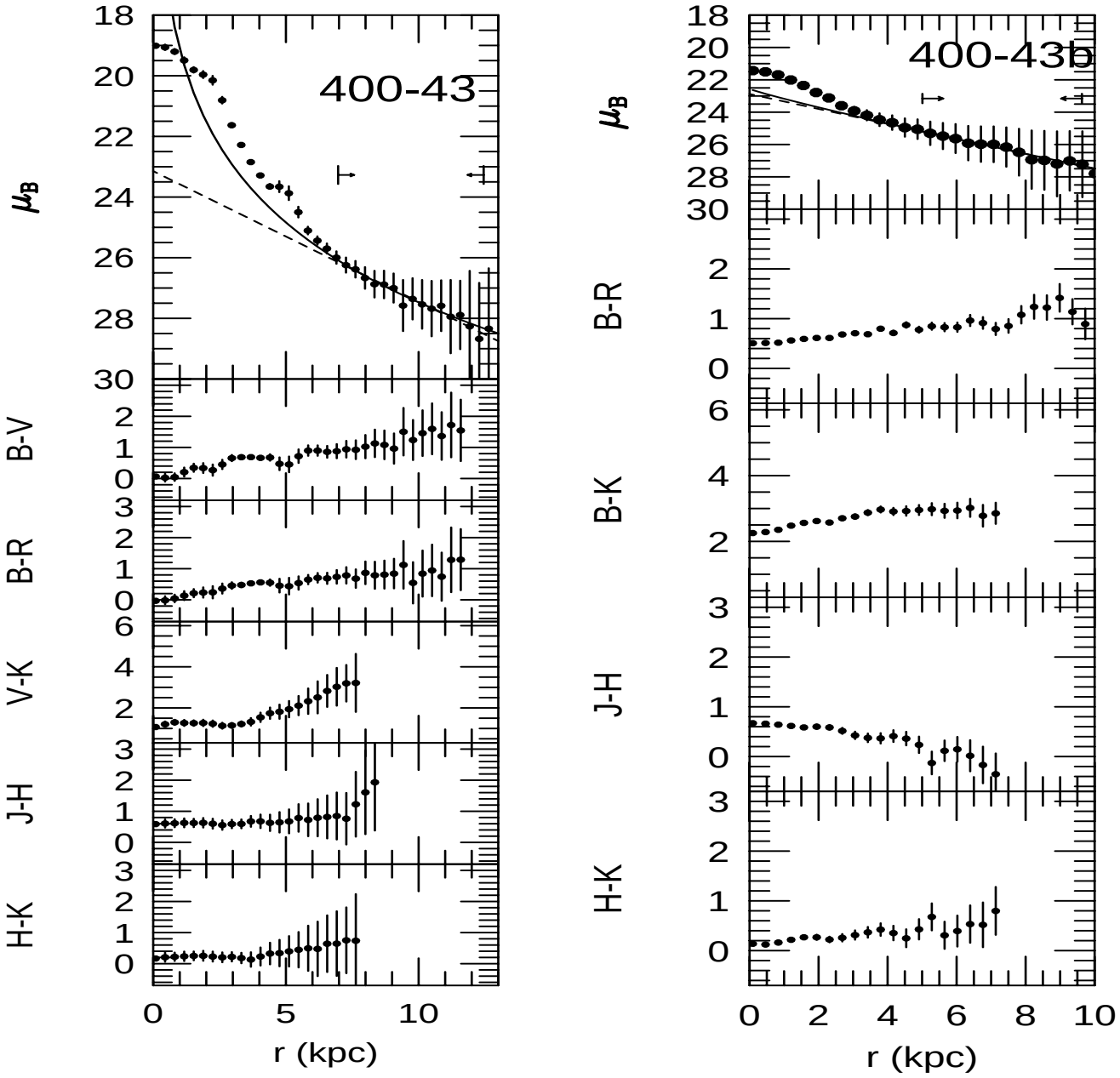

Fig. 16. Luminosity and colour index profiles of ESO 400-G43 and ESO 400-G43b.

is ionised by the central starburst. It is also possible that the expelled gas from the central star forming regions is energetic enough to contribute significantly to the ionisation either mechanically or by conduction. Considering the current debate about what is driving the reionisation of the post-recombination universe it is quite important to identify what is the major important ionising source in luminous BCGs to see if they possibly can contribute significantly to this process.

It seems unlikely that this gas is ionised by stars in situ because we see no support of the presence of young star clusters in the region and the large scale morphology in Hα differs from that of the broadband colours (Fig. 5). We have argued that shocks are important ionisation sources, at least close to the central region. It is hard to say how much outflows may contribute to the ionisation at larger distances but the heat input is probably of importance (e.g. Heckman et al. 2001).

Nevertheless we will now also ask whether it is possible for the young starburst to ionise a halo which has an extent several times larger than the starburst. We made a calculation to the first approximation of how realistic such a situation would be assuming that the gas is in pressure equilibrium and approximately spherically distributed. The density distribution was assumed to follow King's approximation

$$n(r) = n(0)\left(1 + \left(\frac{r}{a}\right)^2\right)^{\frac{-3\beta}{2}} \quad (5)$$

where a is the core radius and β is a constant $\approx$1. As core radius we used the typical value of r_e derived from the profile fits, i.e. $r_e \sim 1$ kpc. From the SEMs, based on a Salpeter mass function with a mass range of 0.1 to 120 $\mathcal{M}_\odot$ and an age of 10^7 years, we obtain a Lyman photon production rate of $\log(N_{\rm Lyc}) \approx 54$

Table 5. Parameters of the best fits to the luminosity profiles of the deepest images. Range is the range of the disk within which the fit was made, h is the scalelength of the exponential fit, $\mu_{0,\mathrm{disk}}$ is the central disk surface brightness in mag arcsec^{-2}, $\mu_{0,\mathrm{disk}}$ is the absolute B (V for 338-04b) magnitude of the disk, n is the parameter in the Sersic approximation where $n = 4$ is the de Vaucouleurs law (see text) and $n = 1$ is an exponential disk, r_e is the effective radius, ρ is the correlation coefficient of the fit, σ is the mean error in the correlation coefficient. All these parameters refer to the solid line in figures 16–18. M_pl is the *limiting* absolute B (V for 338-04b) magnitude inside the Holmberg radius of the power law solution, truncated at small radii to the observed surface brightness level. The data are based on luminosity profiles that were corrected for internal extinction as described in the text.

Galaxy	Filter	Range (kpc)	h_disk (kpc)	$\mu_{0,\mathrm{disk}}$	M_disk	ρ	σ	n	r_e (kpc)	μ_0	ρ	σ	M_pl
338-04	B	6–11	3.3	24.6	−16.6	0.968	0.008	9.8	0.921	1.09	0.973	0.005	−17.7
338-04b	V	6–9	2.4	24.6	−15.9	0.54	0.12	19.8	8.8e-4	−39.39	0.55	0.11	−17.5
350-38	B	8–16	3.2	23.5	−17.6	0.978	0.009	19.8	3.2e-5	−53.95	0.982	0.008	−20.0
400-43	B	6–12	2.5	23.1	−17.5	0.981	0.010	17.1	4.2e-4	−38.85	0.985	0.008	−19.5
400-43b	B	5–9	2.3	22.9	−17.5	0.978	0.014	1.1	3.76	22.54	0.978	0.014	−17.4
480-12	B	6–11	2.4	22.8	−17.7	0.988	0.006	19.7	9.0e-5	−49.18	0.996	0.002	−19.3

for a young metal-poor (10% solar) starburst with a luminosity typical of our target galaxies. The energy balance requirement then allows the ionised gas to reach a radius of 100 kpc within the normal range (e.g. Copetti et al. 2000; Martin 1997) of the filling factor and central density ($f = 0.01$–0.1 and $n_{\mathrm{e},0} = 10$–$100\ \mathrm{cm}^{-3}$). Thus the starburst would be capable of ionising the halo out the region we are exploring.

From our observations we can set limits on the amount of possible excess radiation from nebular emission in the halo and how much it contributes to the light. We have used Hα as a probe to make reasonable estimates. For ESO 338-IG04 we constructed a $W_{\mathrm{H}\alpha}$ map using as continuum a 2000s deep exposure in an Hα narrowband (60 Å) filter designed for a different redshift. The result, Fig. 7), was first discussed in Sect. 4.2.1. Here $W_{\mathrm{H}\alpha}$ drops below 10 Å in the centre. For ESO 350-IG38, we used the deep R image as "off-line" to reach a sufficiently faint surface brightness level. Figure 8 (also discussed in Sect. 4.2.3) shows the resulting $W_{\mathrm{H}\alpha}$ map. As is seen, $W_{\mathrm{H}\alpha}$ stays at a low level in the halo. Similarily, as discussed before in Sect. 4.2.4, Fig. 9 shows $W_{\mathrm{H}\alpha}$ of ESO 400-G43. We notice rather high values on the northeastern side. For ESO480-IG12 we do not have access to a deep Hα image so here we use a slit spectrum. Figure 10 shows $W_{\mathrm{H}\alpha}$ along a slit in the major axis position. We conclude that also in this case $W_{\mathrm{H}\alpha}$ stays at a moderate level, around 50–100 Å although there may be tendencies for an increase at larger distances.

We have modelled the colours and fluxes of a pure HII region in the different wavelengths bands to obtain estimates of how much the nebular emission will contribute to the different wavelength bands as the starburst evolves. Figure 17 shows the relative contribution of the nebular emission to the total emission from stars and ionised gas. Since Hα dominates the emission in the R window we can compare the nebular contribution in the R window with the other wavelength bands and then scale with Hα to obtain the actual contributions. The effective band width of the Cousins R window is ∼1200 Å. Thus, following the results from the spectroscopy and the narrowband images, which indicated $W_{\mathrm{H}\alpha} \leq 100$ Å, we find that the contribution from nebular emission to the total flux in any of the *BRIJHK* windows is <10% and <15% for V. This will have a small but not insignificant effect on the broadband colours when we compare the observations with the predictions. Below we will return to a discussion about to what extent these data can be used to constrain the total emission from the outer parts of the halo.

6. Ages and metallicities – model comparisons

We will now use the colours of the burst and halo regions together with the spectral evolutionary models (SEMs) to constrain the age and metallicity of the stellar populations. The predicted colour evolution of the SEMs depend on the assumed initial mass function (IMF), metallicity and a parameter describing how the SFR changes with time. More sophisticated models also include metallicity evolution and gas flows. There is still on going debate about the slope of the IMF and its possible universality, but within the range consistent with observations (e.g. Salpeter, Scalo, Kroupa et al., Miller-Scalo etc.), varying the IMF has a relatively small impact on colours, except at the very earliest stages. This is because the emitted light will be dominated by the most luminous stars still alive. Sometimes, IMFs truncated at low stellar masses have been proposed for starburst regions. However, at low ages, low mass stars are insignificant contributors to the emitted light, whereas at high ages they are needed to get any light at all. Hence varying the IMF, and its lower and upper mass limits, will affect the mass to light ratio, but have rather small impact on the colour evolution of a stellar population. On the other hand, metallicity and the temporal behaviour of the SFR has a major impact on colours. Assuming that the SFR is constant in time leads to blue colours at high ages, as compared to a short burst. A correct treatment of nebular emission is crucial at low ages, but less important a high ages. Hence, in order to restrict the parameter space, we have chosen to use only models with a "normal" Salpeter IMF, but instead let the metallicity and star fomation history vary and also and the density, covering factor and filling factors of the ionised gas (with a single, observationally

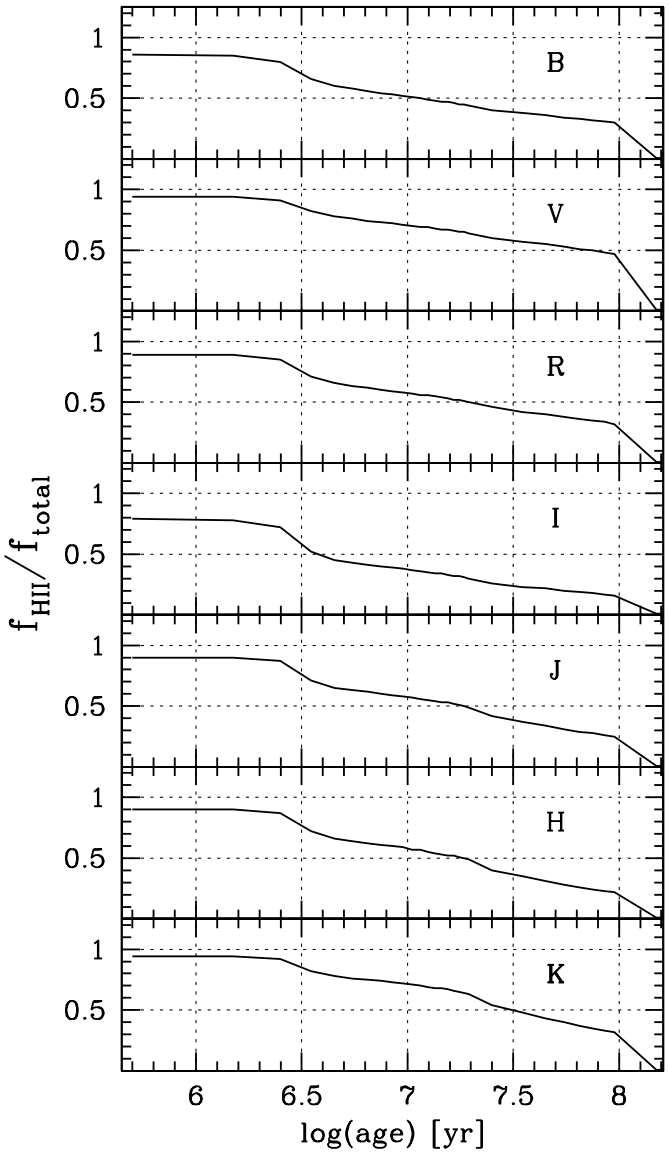

Fig. 17. The relative contribution from nebular emission to the total emission (stars+gas) in different broadband windows. The colours are based on a model of a continuous star formation rate with a Salpeter mass function and a metallicity of 5% solar.

known, metallicity). In Table 6, we give a list of the used parameters in the SEMs.

6.1. Location in the $B-V$ vs. $V-K$ diagram

Before entering into the detailed modelling of the halo colors, we will have a look at the location of the galaxies in the $B-V$ vs. $V-K$ two colour diagram. In Figs. 18, 19, 20 and 21 we try to show, as simple as possible, the main restrictions we can impose on the stellar populations in the galaxies. The $V-K/B-V$ diagrams show the predicted colour evolution from 0 to 14 Gyr of a star forming galaxy with different star formation histories and metallicities. For comparison we show the results from three different SEMs from three different research groups.

In Fig. 18 we show the predicted evolution of an exponentially decaying star formation history with timescale of 1 Gyr at two different metallicities, 5% solar and twice solar (Zackrisson et al. 2001). Figure 19 shows the same data with the difference that the star formation decay rate is now 14 Gyr. Hence these represent 4 extreme cases, and the truth may well lie in between. An instant burst model would differ from the $\tau = 1$ Gyr model, only for ages less than a few Gyrs. However, real galaxies can hardly be truly instantaneous on a global scale, but a time scale of 1 Gyr is probably more realistic. In Fig. 18 ($\tau = 1$ Gyr) one sees that the the colours of the starburst regions seem to fall along the metal-poor track, whereas, surprisingly (given the observed nebular metallicities), the halo colours lie close to the old ages of the metal-rich track. The same pattern is seen Fig. 19 ($\tau = 14$ Gyr), but now the two reddest halos are redder than even the oldest points in

Table 6. Model parameters of the fit to the spectral evolutionary model of Zackrisson et al. (2001) SFH, the star formation history, is assumed to be of two types: constant (const) or exponentially declining (expo). Z is the metallicity. τ is either the duration of the burst or the e-folding timescale of the SFR. n_e is the electron density of the nebular component, f is the filling factor of the ionised gas and c is the covering factor of the ionised gas, i.e. the relative amount of nebular emission to the stellar light responsible for the ionisation.

Model set no.	Model no.	SFH	Z	τ (Myr)	n_e cm^{-3}	f	c
1	1	const	0.001	14000	100	1	1
	2	const	0.001	10	100	1	1
	3	const	0.001	100	100	1	0.5
	4	const	0.001	100	100	0.1	1
	5	const	0.001	100	1	0.1	0.5
	6	const	0.001	100	1	1	1
	7	const	0.001	100	100	1	1
	8	expo	0.001	14000	100	1	1
	9	expo	0.001	1000	100	1	1
2	1	const	0.001	1400	100	1	1
	2	const	0.001	10	100	1	1
	3	const	0.001	100	100	1	0.5
	4	const	0.001	100	100	0.1	1
	5	const	0.001	100	1	0.1	0.5
	6	const	0.001	100	1	1	1
	7	const	0.001	100	100	1	1
	8	expo	0.001	14000	100	1	1
	9	expo	0.001	1000	100	1	1
	10	const	0.004	14000	100	1	1
	11	const	0.004	10	100	1	1
	12	const	0.004	100	100	1	1
	13	const	0.004	100	100	1	0
	14	expo	0.004	14000	100	1	1
	15	expo	0.004	1000	100	1	1
	16	const	0.020	10	100	1	1
	17	const	0.020	100	100	1	1
	18	const	0.020	100	100	1	0
	19	expo	0.020	14000	100	1	1
	20	expo	0.020	1000	100	1	1
	21	const	0.040	10	100	1	1
	22	const	0.040	100	100	1	1
	23	const	0.040	100	100	1	0
	24	expo	0.040	14000	100	1	1
	25	expo	0.040	1000	100	1	1

Table 7. Halo broadband colours and fits to the spectral evolutionary model. The table shows the integrated colours of the outermost region containing useful near-infrared data and the best model fit to the data. The model is based on two stellar components, one which is assumed to have a metallicity of 5% solar (the first model of the two). The metallicities of the second component ranged from 5% to twice solar. The allowed age range was 0 to 15 Gyr. A Salpeter IMF was assumed. The model numbers refer to the numbers in Table 6. The fits were made by mixing the spectral distributions of two models, one from each of the two groups in the table, giving them weights that minimized the deviation from the observations. Among these, the mix that resulted in the best fit to the data was finally selected and presented below. The table shows the colours, total M_V/L ratios (i.e. including dark baryonic matter) and masses of the two components and the mixture between the two. $\Delta_{\rm Halo-Mix}$ is the difference between the observations and the model predictions. The masses were calculated from the estimated halo luminosity based on the power law fit in Table 5. At the end of respective row σ is the weighted mean error of the observed colours and the fits and $\sigma_{\rm mp}$ is the weighted mean error of the best fit when only metal-poor ($\leq$20% solar) models were used.

Galaxy	Component	Age (yr)	M_B	$B-V$	$B-R$	$V-I$	$V-K$	$J-H$	$H-K$	M_V/L	Mass ($\mathcal{M}_\odot$)	σ mag	$\sigma_{\rm mp}$ mag
338-04	Halo		−17.70	0.31	0.69	0.70	2.83	0.68	0.12				
	$\sigma_{\rm obs}$		0.02	0.03	0.03	0.05	0.24	0.36	0.35			0.017	
	Model 1	4.5e8	−16.24	0.17	0.13	−0.06	0.67	0.25	0.15	0.16	5.0e7		
	Model 24	7.5e9	−17.36	0.39	0.85	0.88	2.73	0.57	0.25	2.35	2.5e9		
	Mix		−17.69	0.34	0.70	0.73	2.50	0.56	0.25	1.85	2.6e9		
	$\Delta_{\rm Halo-Mix}$		−0.01	−0.03	−0.01	−0.03	0.33	0.12	−0.13			0.017	0.032
338-04b	Halo		-	-	-	0.62	2.87	0.42	0.41				
	$\sigma_{\rm obs}$		-	-	-	0.03	0.28	0.17	0.28			0.02	
	Model 9	5.0e5	−16.95	0.63	0.00	−1.46	−0.22	0.04	0.58	0.005	4.6e6		
	Model 22	6.5e9	−16.55	0.94	1.63	1.34	3.55	0.64	0.28	7.39	6.3e9		
	Mix		−17.52	0.77	0.96	0.63	2.79	0.62	0.29				
	$\Delta_{\rm Halo-Mix}$		-	-	-	0.00	0.08	−0.20	0.12			0.01	0.13
350-38	Halo		−20.00	0.87	1.24	-	4.16	-	0.82				
	$\sigma_{\rm obs}$		0.03	0.26	0.12	-	0.81	-	1.20			0.21	
	Model 9	5.0e5	−19.16	0.63	0.00	−1.46	−0.22	0.04	0.58	0.005	3.5e7		
	Model 23	14.5e9	−19.33	1.02	1.76	1.46	3.77	0.66	0.28	14.92	1.8e11		
	Mix		−20.00	0.86	1.26	1.00	3.28	0.65	0.28	9.35	1.8e11		
	$\Delta_{\rm Halo-Mix}$		0.00	0.01	−0.02	-	0.88	−0.65	0.54			0.09	0.22
400-43	Halo		−19.50	0.92	0.74	-	3.15	0.95	0.71				
	$\sigma_{\rm obs}$		0.03	0.19	0.19	-	0.78	0.63	0.86			0.13	
	Model 6	5.0e5	−19.15	0.65	−0.03	−1.50	−0.25	0.04	0.58	0.005	3.6e7		
	Model 22	13.5e9	−18.10	1.02	1.76	1.46	3.76	0.66	0.28	13.59	5.2e10		
	Mix		−19.50	0.76	0.80	0.44	2.66	0.63	0.29	4.73	5.2e10		
	$\Delta_{\rm Halo-Mix}$		0.00	0.15	−0.07	-	0.48	0.31	0.42			0.14	0.31
400-43b	Halo		−17.40	-	0.89	-	*2.88*[1]	−0.17	0.62				
	$\sigma_{\rm obs}$		0.05	-	0.09	-	*0.22*[1]	0.26	0.31			0.12	
	Model 4	2.5e9	−17.28	0.41	0.78	0.70	*2.24*[1]	0.41	0.13	1.76	1.8e9		
	Model 22	10.5e9	−14.97	1.00	1.73	1.43	*4.72*[1]	0.65	0.28	10.76	2.2e9		
	Mix		−17.40	0.49	0.93	0.86	*2.96*[1]	0.53	0.21	3.30	4.1e9		
	$\Delta_{\rm Halo-Mix}$		0.00	-	−0.04	-	−0.08	−0.70	0.41			0.16	0.19
480-12	Halo		−19.30	0.51	0.79	-	2.67	0.93	−0.38				
	$\sigma_{\rm obs}$		0.03	0.13	0.09	-	0.54	0.31	0.56			0.14	
	Model 9	3.5e7	−18.90	0.26	−0.04	−0.61	0.05	0.12	0.29	0.03	9.8e7		
	Model 23	14.5e9	−18.01	1.02	1.76	1.46	3.77	0.66	0.28	14.92	5.2e10		
	Mix		−19.29	0.55	0.87	0.81	2.99	0.64	0.28	7.05	5.2e10		
	$\Delta_{\rm Halo-Mix}$		−0.01	−0.04	−0.08	-	−0.32	0.30	−0.66			0.11	0.32

1) The data refer to $B-K$ instead of $V-K$.

the metal-rich model. Hence, this first simple look at the halo colours suggests that the halos are old, metal-rich and formed on relatively short timescales.

In Fig. 20 we use the predictions from the PEGASE2 model (Fioc & Rocca-Volmerange 2000), in which the recycling of metals in a closed box scenario have been taken into account. Two tracks are displayed – one shows the evolution of a stellar population with zero initial metallicity assuming the star formation rate is kept constant. The other track shows the evolution starting from an initial metallicity of approximately 5% solar ($Z = 0.001$) and then evolving with an exponentially declining SFR and a decay rate of 1 Gyr, as in Fig. 18. In this diagram we also display the predictions of colours of an old stellar population of 3 different metallicities ([Fe/H] = $-1.0, 0.0$ and

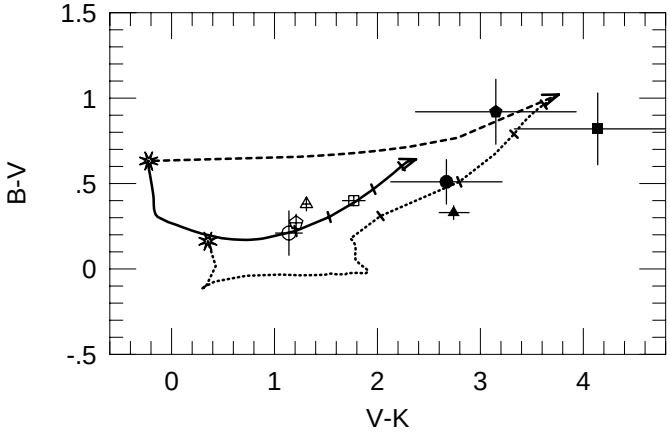

Fig. 18. The predicted evolution of $B-V$ and $V-K'$ of of a star formation galaxy with an e-folding decay rate of 10^9 years. Two scenarios (models no. 1:9 and 2:25 in Table 6) with different metallicities, 5% solar (solid line) and twice solar (dotted line), are shown. A Salpeter mass function is assumed. The burst starts at the stellar symbol and ends after 14 Gyr at the arrows. The hatches along the evolutionary tracks mark the evolution at 1, 2, 4 and 8 Gyr. The hatched line indicates the theoretical position of a young burst superposed on the old metal-rich population if we continuously vary the relative contribution of the burst to the integrated light from 0 to 100%. Data for the central burst (unfilled symbols) and and the halo (filled symbols) of the target galaxies are shown. The galaxies are ESO 338-IG04 (triangle), 350-IG38 (square), 400-G43 (pentagon) and 480-IG12 (circle). Reddening corrections based on spectroscopy of the central region and assuming the column density of the dust to be proportional to the luminosity density, have also been applied.

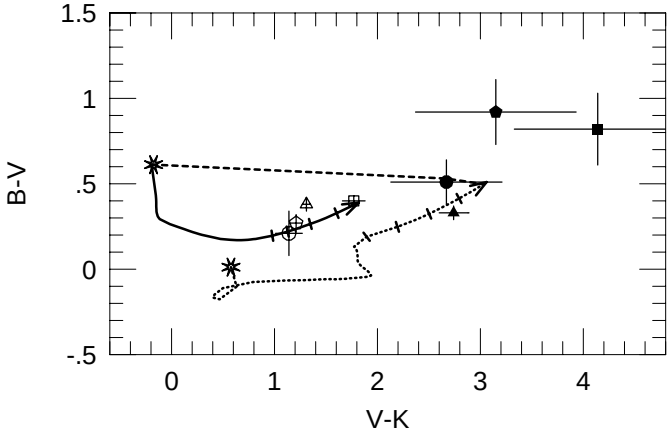

Fig. 19. Similar to Fig. 18 with the difference that the decay rate of the star formation is 14 Gyr (models 1:8 and 1:24 in Table 6).

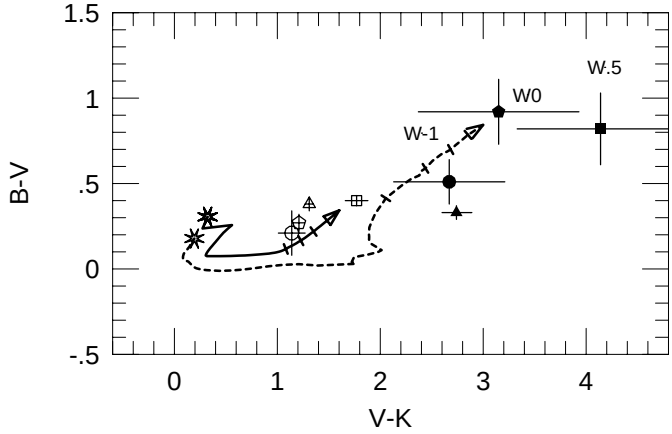

Fig. 20. The diagram shows the predicted evolution from the PEGASE model (Fioc & Rocca-Volmerange 2000) in $B-V$ and $V-K'$ of a star forming galaxy with constant star formation rate and zero initial metallicity (full drawn line) and a constant star formation rate during the initial 10^8 years and an initial metallicity of 5% solar ($Z = 0.001$; hatched line). The bursts start at the stellar symbols on the left and end after 14 Gyr at the arrows. The final mass weighted stellar metallicities are about 10% solar and 1.2 times solar respectively. Also indicated are the predicted colours from Worthey (1994) of an old (12 Gyr) single-burst stellar population of three different metallicities, [Fe/H] = −1.0, 0.0 and 0.5. These are indicated by the symbols W-1, W0 and W05 respectively. The observational data are displayed as in Fig. 18.

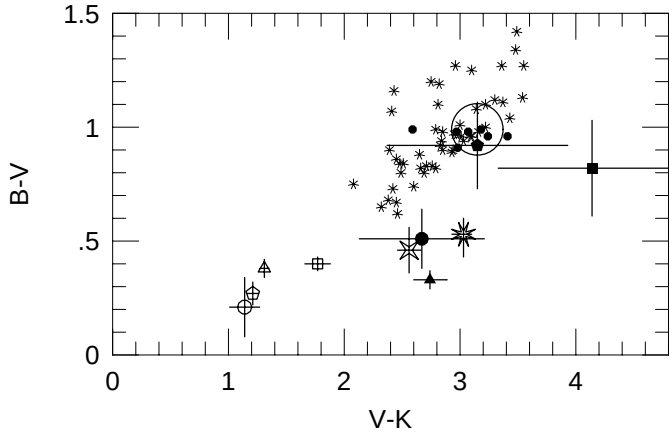

Fig. 21. The observed colours of isolated E/S0 galaxies (Bergvall & Johansson 1995; filled dots), M31 globular clusters (Barmby et al. 2000; stars), the mean position of local ellipticals (Pahre 1999; large circle), the disk of the luminous LSBG 0237-0159 (Bell et al. 2000; big star), the low luminosity elliptical ESO 118-G34 (Sadler et al. 2000; diamond). Our BCG data are displayed as in Fig. 18.

0.5) from Wortheys (1994) models. On top of this we display the colours of the central region and the halo of our BCGs. Again, it appears that the reddest halos are old and quite metal-rich.

As can be seen, the colours of the central starburst agree very well with the predictions from the metal-poor model. An important fact to remember is that all 4 BCGs show Wolf-Rayet features in their spectra and have strong Balmer emission lines and thus must contain a considerable fraction of very young stars, as is also indicated by the photometry in the UV/blue region and UV spectra obtained with IUE. What may seem somewhat unexpected perhaps is that the luminosity weighted ages of the burst populations, as found from the positions in the diagrams, are quite high, as if the star formation has been going on continuously for more than 1 Gyr. This cannot be correct because it is not consistent with the high equivalent widths of the observed emission lines. The equivalent width of Hα is several

hundred Å and the luminosities correspond to star formation rates of several $\mathcal{M}_\odot$ yr^{-1}. The available gas budget of a few times $10^8 \mathcal{M}_\odot$ would be thus consumed in about 10^8 yr (or even faster if we have a decaying SFR) unless the IMF is peculiar. The explanation of the colours is probably that there is a burst occurring in an old host. In Figs. 18 and 19 we show the effect on the colours of the transition from a passive old population to a young burst. Depending on the age and the relative mass of the burst it may take any position within the region defined by the connecting lines between the young and old population. Although the optical region may be little affected by the mixing of the two population we may notice it in the near-IR, in $V-K$. A mixed population with 10% of the V-band luminosity from a population with the same color as the ones observed in the halos and a 90% from a young (10^7 yr) model population gives composite colors which agrees well with those of the central regions. Thus it is perfectly proper to assume that the ages of the burst population are quite low, i.e. ≤10 Myr.

6.2. Best fitting models to the halo colours

Let us now look a bit more detailed at the spectral energy distribution of the halos and the best fitting SEM predictions from the Zackrisson et al. (2001) model. For simplicity and considering the large uncertainty in the near-IR colours of the halo, a few parameters of the SEMs were kept fixed. Thus we assumed a Salpeter IMF, a mass range between 0.08 and 120 $\mathcal{M}_\odot$ and a constant metallicity.

We mixed two models where the metallicity in both gas and stars in one of the models was fixed to 5% of the solar (set No. 1 in Table 6). We think this is a reasonable guess of the metallicity of the gas used in the burst. It is also at the lower envelope of the metallicity of the (recently enriched) ISM of gas-rich LSB galaxies which, as we will argue below, are attractive merger candidates. Hence this metal-poor component would allow us to simulate contamination to the halo colours from young stars. The metallicity of the second component, which we may associate with the halo population, was allowed to vary between 5% solar and twice solar (set No. 2 in Table 6). The star formation rate was either assumed to occur in a burst of constant SFR for $t \leq \tau$ or in an exponentially declining mode, SFR $\propto \mathrm{e}^{-\frac{t}{\tau}}$, where t is the age of the burst and τ is the duration of the burst or the SFR decay timescale. Table 6 lists the parameters of the models we included in the comparison. The optimized mixture of the two sets of models were fitted to the observed fluxes that were given weights in proportion to the square of the inverse of the mean error.

Table 7 lists the models that, when optimally mixed, gave the best fits to the observed broadband fluxes. The table displays predicted colours and the deviations from the observations. Also inluded are the weighted mean errors of the observations and the mean error of the fit. The errors refer to the colours and are based on the weighted errors of the fits to the fluxes. Although the errors are quite large (we are investigating regions with very low surface brightneses), the best fits are with a few exceptions obtained within about 1σ of the observational errors. It is noteworthy that we find several cases of large deviations with respect to the observed $V-K$ colours, in the sense that observations are redder than the models. Hence, increasing the weight of the near IR data would lead to higher ages and metallicities. The extremely young ages derived for the metal-poor component in 2–3 cases is of course unrealistic and should be regarded as indications of low age only. The important result is that, even as we include all available photometry in the comparisons, we get consistency with the conclusions from the previous discussions – the halo components of *all galaxies* have colours that best fit with models of an *old metal-rich stellar population*.

For comparison, we have also included in the table the mean error of the best fit to a model including only metal-poor (<20% solar) stellar populations. These fits are significanlty worse except for one case, ESO 400-G43b. In this case the fit is equally good if we assume a low metallicity throughout. It is interesting to note that this is also the only galaxy in our sample that has a luminosity profile that fits well with an exponential disk. It thus has properties similar to LSB galaxies that are thought to have had a rather constant and low star formation activity over a long time and are probably not sitting in massive halos. The other cases typically deviate with 1–3σ from the observations and are thus 2–3 times worse when we force the halo to have a low metallicity. While the errors are large, and the sample is small, the comparison with the SEMs suggest that the halos are more metal-rich than inferred from the nebular gas.

The predicted photometric masses of the halos, based on the halo luminosities from Table 5, range from 3×10^9 to 2×10^{11} $\mathcal{M}_\odot$ and should be regarded as upper limits. Had we chosen the Scalo (1998) IMF instead of the Salpeter IMF, the predicted masses would be reduced with a factor ≈2. Moreover, had we used an exponential luminosity profile in estimating the the total halo luminosities, the mass estimates would go down with up to a factor of 10.

7. Discussion – Evolutionary scenarios

Now let us have a look at the halo colours and discuss the properties of the host of the starbursts. Let us first recall the most popular alternative star formation scenarios discussed in this context: 1) What we observe is the first star formation epoch in the history of the galaxy. The galaxy is young. 2) This is one of several intermittent bursts taking place in the galaxy. The bursts are caused by infall of cooled gas from the halo, processed in a previous burst. 3) Interaction with a neighbor, causing gas from the outskirts to fall towards the centre, thereby igniting a burst 4) Merger between galaxies or one galaxy (or a few galaxies) and intergalactic gas clouds. We will now discuss these alternatives one by one.

7.1. Young galaxy

The fact that the chemical abundances are low and homogeneous agree with a young galaxy but the colours and the morphology of the halo population do not. We have shown that the light from the halo is dominated by stars. Thus the galaxy has to be at least as old as the time it takes for the stars to relax into

a regular structure. This is at least a few crossing times or a few hundred Myr. The colours of the halo populations are much redder than that of metal-poor gas-rich low surface brightness galaxies (BCG halo: $B-J = 2.6 \pm 0.2$ mag. as compared to LSB: $B-J = 1.5 \pm 0.2$ mag.; Bergvall et al. 2000) and do not at all agree with a young metal-poor population. The agreement is fine however, with a *metal-rich stellar population of an intermediate-high age (≈2–15 Gyr)*. This is evident from the figures where the model predictions are displayed and is consistent with all three model codes we compare with. Both ESO 350-IG38 and 400-G43 appear to have old halos while ESO 338-IG04 and 480-IG12 may have halo ages of between 1 Gyr and a Hubble age, depending on the contribution of young stars to the halo light.

In Fig. 21 we compare with different samples of observational data from the literature. This includes a set of globular clusters in M31 (Barmby et al. 2000) a sample of seemingly isolated E/SO galaxies (no bright neighbors in projection; Bergvall & Johansson 1995) and another sample of mostly cluster ellipticals (Pahre 1999), the distribution of which is indicated by a large circle in the diagram. The range of metallicities of the globulars is $-2.0 \leq$ [Fe/H] ≤ 0, with mean metallicities slightly below [Fe/H] $= -1.0$. This is close to the metallicity of the burst population of our target galaxies. Yet they deviate strongly from the colours of the halos. This is in disagreement with Doublier et al. (2001). They however studied the global colours and their sample was selected differently. Admittedly the error bars of the halo colours are quite large but taken together we find no other reasonable explanation than high age and high metallicity (taking the risk of generalizing the properties of the halos of the four galaxies). We have no reason to suspect that we have serious calibration problems and a comparison with the few other photometric data available is reassuring. E.g. our photometry of the galaxy with the most extraordinary colours, ESO 350-IG38, agree remarkably well with those of Vader et al (1993). They obtain $M_B = -20.2$, $K = 12.08$, $J-H = 0.62$, $H-K = 0.62$ ($D = 9.3''$) We obtain $M_B = -20.0$, $K = 12.06$, $J-H = 0.67$, $H-K = 0.62$.

7.1.1. Gas and dust emission

In Sect. 6 we concluded that the influence of gas and dust on the colours is small. How much and in which direction would the colours be affected if we relax these constraints? We have discussed some constraints on the Hα emission that cover the region including the infrared data of ESO 350-IG38, 338-IG04 and 400-G43. In these two cases we can rather safely say that the contribution from nebular emission to the halo light is negligible. But in the other cases we cannot exclude that the contribution from nebular emission increases as we reach the red regions. It is therefore motivated to have a look at how nebular emission would affect the colours. We can derive the colours of a pure HII region (i.e assuming no stars in the halo so that 100% of the flux is due to the ionised gas) assuming that the metallicity is the same as that of the ionised gas in the centre. The colours we obtain are $B-V \leq 0.74$ and $V-K \leq -0.17$, i.e. significantly bluer than observed. Thus, if anything, the colours of the stellar population would become redder if we correct for the contribution from emission from gas ionised by the central source. With the assumptions made in Sect. 6 the correction in $B-V$ would be marginal while in $V-K$ it would amount to 0.1–0.2 magnitudes.

Could the emission be due to warm dust? We may constrain the properties of such a component from the K band photometry combined with ISOCAM 4–14μ data of ESO 350-IG38 from the ISO mission (Bergvall et al., in preparation). The total fluxes we obtain from the ISOCAM data are 4.0μ: 23.6 ± 0.3 mJy, 6.7μ: 70.6 ± 0.4 mJy, 9.6μ: 151 ± 1 mJy, 14.3μ: 589 ± 3 mJy. If we assume an emissivity of $\epsilon \propto B_\nu \lambda^{-\beta}$, with $1.4 \leq \beta \leq 2.0$ (Lisenfeld et al. 2000) we obtain a temperature range of 100–160 K based on these global ISO data. If the heating is caused by the central burst, 160 K is the maximum temperature we can accept in the halo. The total K band flux density is 135 mJy. 10% of this emission originates from the region outside 5 kpc that has a clear red excess. The excess in K' relative to a metal-poor stellar population is $\sim 1.4^m$, or roughly 80%. If we therefore assume that at least 50% of the K' emission, i.e. ~7 mJy, comes from warm dust we can calculate a *minimum* temperature of the dust from the 2μ and the 4μ fluxes. The 4μ emission outside 5 kpc contributes with ~5% of the total emission in this frequency band. With these data, the temperature we derive is around 3500 K, which is impossible if the dust is heated by the central burst and unreasonable if the dust is heated in situ. Warm circumstellar dust with a temperature of 500 K would contribute with 0.1% of the K flux from the halo if we scale it with the 4μ emission. We conclude that the contribution from dust emission to the halo K' luminosity is insignificant.

Since the dust extinction to the amount that would be needed for the data to be consistent with a young age, i.e. $A_B \sim 1$ mag, probably can be excluded, the only alternative remaining, if we stick to low metallicities, is that the IMF is odd. But, if so, the only option is a very low upper mass limit, a highly improbable situation if we can trust the theoretical models of star formation. The youth hypothesis therefore can be dismissed.

7.2. Recurrent bursts

We have shown in a previous paper (Östlin et al. 1998) that at least ESO 338-IG04 has been involved in previous bursts. But if the gas in the present burst originates from expelled gas from a previous burst, the metallicity of the gas must be higher than or comparable to that of the host, not an order of magnitude lower. Following the conclusions from the previous discussion, this is not the case. We can therefore conclude that recurrent bursts, controlled by the cyclic expulsion and later accretion of the ISM, cannot be the explanation of the starburst seen in our BCGs. Previous bursts induced by infall of fresh material, either from gas-rich dwarfs or in the form of intergalactic HI clouds, are however not excluded.

7.3. Tidally induced burst

Gas rich galaxies of low to intermediate masses have small abundance gradients. Thus if the starburst is caused by interaction with a neighboring galaxy we still would have to explain why the metallicity of the gas is lower than that of the old stars. Moreover the statistics give no observational support of strong starbursts caused by interaction between low mass galaxies. Only gas-rich LSB galaxies have the required properties of the metal-poor progenitor and it seems to be very difficult to ignite a starburst in such a galaxy (Mihos et al. 1997).

7.4. Merger

A merger between two galaxies of different metallicities, one gas-rich and one gas-poor, or infall of intergalactic clouds, appear to be the most plausible explanation of the observational results. We have argued in previous papers (Bergvall et al. 1998, 2000) that gas-rich LSB galaxies, and perhaps only this type of galaxy and not normal irregulars, have the required properties of the metal-poor component. One of the arguments was based on the location of these galaxies in the metallicity–luminosity diagram (Fig. 12). If one assumes the progenitor to be a dI, the offset of more than 3 mag in luminosity from the dI relation would require an excessive neutral hydrogen gas mass. LSBGs on the other hand already lie offset from the dI relation, meaning that they need to brighten less, and in addition, the gas mass fractions are much higher than for dIs. Note that also IZw18 and SBS 0335-052 show the same offset from the $M_B - Z$ relation in Fig. 12.

The old halo component could be a dwarf elliptical, a massive ellipsoidal disk or a similar type of galaxy. If the last interpretation is correct, it would indicate that there should be cases in which we would find low luminosity early type galaxies hosting HI clouds or gas-rich galaxies in a state prior to a burst. Sadler et al. (2000) observed four E/S0 and S0 galaxies with these properties. Their sample galaxies have luminosities ranging from $M_B = -17.0$ to -19.1, i.e. similar to the maximum luminosities of our host galaxies, and contain HI with masses in the range 10^8 to 10^9 $\mathcal{M}_\odot$. They found that the HI is strongly concentrated towards the central region, differing from what is found in normal early type galaxies. In two of the cases the distribution of the HI resembles warped disks like in ESO 338-IG04 and ESO 480-IG12. Similar results were obtained by Lake et al. (1987) for another sample of low luminosity early type galaxies. James & Mobasher (1999) find star formation activity most frequent in ellipticals situated in regions of low density but not completely isolated. Two of the galaxies in the Sadler et al. sample show clumpy HII emission in the centre with an Hα luminosity about a few percent of what we observe in our BCGs. Interestingly enough, the optical/near-IR colours are similar to the halos of our disk-like systems, e.g. their ESO 118-G34 has the colours $B - V = 0.46$ and $V - K = 2.56$, similar to the halo of ESO 480-IG12 ($B - V = 0.51$, $V - K = 2.67$). It is also interesting that the halo colours of ESO 338-IG04 and 480-IG12 agree with the disk colours of a giant LSB galaxy observed by Bell et al. (2000), believed to have supersolar metallicities from their comparison with SEMs. The positions of these galaxies have been indicated in Fig. 21.

7.5. Host galaxies and dark matter

It seems that the best candidate of the starburst host galaxy in our BCGs is a galaxy of early morphological type. We know that dEs have the highest fraction of dark matter of all galaxy types and that the DM density is extremely high, approximately 1000 times higher than in large ellipticals. Here we have the preconditions needed for creating dynamical instabilities in an infalling LSB disk, followed by inflows and a starburst. But there is also another alternative. Massive ellipticals may form in the gravitational wells of large amplitude dark matter fluctuations. In the early formation phase they consequently were much more dark matter dominated than they are today. In sparse regions the buildup of the stellar component of the galaxies would proceed with a lower tempo and maybe there we could find DM dominated *massive* Es that occasionally would be involved in mergers. A massive DM halo would be more efficient in retaining metals produced in a burst than a low mass one, thus explaining the red colours. Support for mergers or infall taking place in isolated early type galaxies of L^* luminosities ($M_B \sim -20$) comes from e.g. Colbert et al. (2001). They found evidence of recent mergers in about 40% of the cases and in higher proportions than found in richer groups.

Early type galaxies follow a colour-magnitude relationship that may be used to estimate the predicted luminosity of the host, provided it is a normal early-type galaxy. We can for instance use the relationship based on cluster ellipticals or compare to $V - K$ colours derived from models including effects of infall of gas and SN generated outflows (e.g. Gibson 1997; Ferreras & Silk 2000; Fioc & Rocca-Volmerange 2000). The luminosity we would expect for a galaxy with colours similar to the halo colours of our BCG sample is much higher than what we obtain from the photometry. There are at least two possible ways to explain this difference. One is related to the mechanism behind the metallicity-colour-luminosity relationship. This relationship is mostly thought to be caused by the mass dependency of loss of metals through stellar winds. According to the models by Mc Low & Ferrara (1999) and Ferreras & Silk (2000) mass loss from galaxies during a starburst phase is strongly dependent on the mass of the galaxy and dwarfs may, depending on the morphology, lose most of the metals produced in the starburst to the environment. If galaxy formation is biased towards high density regions, it would mean that the field ellipticals contain less baryons per dark matter mass unit, i.e. there would be an anticorrelation between mass-to-luminosity and mean density of the environment. The critical luminosity for mass loss would therefore decrease and we might find low luminosity, metal-rich galaxies in sparse regions. From time to time a gas-rich galaxy would fall into this potential well and start a starburst similar to what we would expect to see at high redshifts. It is interesting to note that the fit to the Sersic equation of the halo luminosity profile that was described in Sect. 4.5, resulted in very high values of the n parameter. Although individually these are quite uncertain

values, these data collectively also indicate that the mass of the host is large. If ther merger hypothesis is valid, further support for massive halos comes from n-body simulations of mergers. Dubinski et al. (1999) found that tidal tails do not develope in disk galaxies where the mass is stongly dominated by the halo. Although we see some morphological signatures of the aftermaths of mergers, we do not see tails.

7.6. A peculiar IMF?

One may also consider the possibility of an abnormal IMF, which drastically could change the interpretation of the colours. More and more evidence is accumulating however in the direction of a universal IMF. While local variations may occur, the global properties closely agree with the classical Salpeter IMF (Scalo 1998). On the other hand there are strong biases in IMF studies since they normally deal with star forming regions that are luminous and the star formation efficiency is high. The low surface brightness makes it problematic to investigate star formation regions in which the mean density is low, as in e.g. low surface brightness galaxies. Dynamical estimates of the mass and the $\mathcal{M}/L$ ratio are more reliable but also have their limitations because of the uncertainties in inclination, contribution from dark matter and due to distorsions in the velocity field, both in the central area and in the HI distribution. A possible contribution from population III stars with peculiar IMF cannot be excluded as an exotic candidate to explain the red excess.

8. Conclusions

We present the result of an optical/near-IR photometric/spectroscopic investigation of four luminous blue compact galaxies and their companions. The chemical abundances of the BCG starbursts are low, typically 10% of the solar values. The star formation is intense, corresponding to gas consumption timescales of the order of 100 Myr only. We show that the main body is embedded in a huge halo of ionised gas, possibly ionised by the central burst. The galaxies thus have properties we normally associate with young galaxies and one of our targets, ESO 400-G43, is in the list of young galaxy candidates. We conclude however that all galaxies discussed here contain a significant population of old stars.

We demonstrate that is is possible to disentangle a separate "halo population" from the burst population. This very red component has colours and structural properties typical of elliptical galaxies with metallicities considerably in excess of that of those derived from the starburst HII-regions. From this we conclude that the starburst is not an internal affair but is caused by a galaxy merger or infall of gas from the intergalactic space.

In the optical region the galaxy type that dominates the light is typical of gas-rich low surface brightness galaxies. The luminosity of the halo, as derived from the empirical metallicity-luminosity relationship of normal galaxies, is much in excess of what is observed. A possible scenario is that we witness mergers between gas-rich LSB galaxies or massive HI clouds and massive and metal-rich, but extraordinary faint ellipticals. Such galaxies may exist in low density regions as a consequence of a different distribution of baryons and dark matter (the classical bias), causing the field ellipticals to contain relatively more dark matter than the cluster ellipticals. Alternatively the host may have a very peculiar IMF.

The deep dark matter potential field of the Es may be necessary conditions for the burst to start. Our findings may be typical of luminous blue compact galaxies in general and may prove to be important in the early formation of galaxies. Similar starbursts occurring in more luminous ellipticals may be rare because such galaxies have experienced sufficiently many starbursts to build up an extended hot corona of ionised gas that will shield the galaxy from infall of neutral gas by thermal conduction.

Acknowledgements. We thank Saga Dagnesjö, Steven Jörsäter, Kjell Olofsson, Jari Rönnback and Erik Zackrisson for their contributions to this work and for stimulating discussions. This work was partly supported by the Swedish Natural Science Research Council.

References

Alloin, D., Bergeron, J., & Pelat, D. 1978, A&A, 70, 141
Barmby, P., Huchra, J. P., Brodie, J. P., et al. 2000, AJ, 119, 727
Bell, E. F., Barnaby, D., Bower, R. G., et al. 2000, MNRAS, 312, 470
Bergvall, N. 1985, A&A, 146, 269
Bergvall, N., & Jörsäter, S. 1988, Nature, 331, 589
Bergvall, N., & Olofsson, K. 1986, A&AS, 64, 469
Bergvall, N. 1992, Phys. Scr. T43, 67, ed. A. Elvius
Bergvall, N., & Rönnback, J. 1995, MNRAS, 273, 603
Bergvall, N., & Johansson, L. 1995, A&AS, 113, 499
Bergvall, N., Östlin, G., Pharasyn, A., Rönnback, J., & Masegosa, J. 1998, in Highlights in astronomy, proceedings from the X:th IAU general assembly (Kluver)
Bergvall, N., Östlin, G., Masegosa, J., & Zackrisson, E. 1999, Ap&SS, 269/270, 625
Bergvall, N., Masegosa, J., Östlin, G., & Cernicharo, J. 2000, A&A, 359, 41
Brocklehurst, M. 1971, MNRAS, 153, 471
Burstein, D., & Heiles, C. 1982, AJ, 87, 1105
Caon, N., Capaccioli, M., & D'Onofrio, M. 1993, MNRAS, 265, 1013
Capaccioli, M. 1989, in The World of Galaxies, ed. H. G. Corwin, & L. Bottinelli (Springer, Berlin), 208
Clegg, R. E. S. 1987, MNRAS, 229, 31
Colbert, J. W., Mulchaey, J. S., & Zabludoff, A. I. 2001, AJ, 121, 808
Copetti, M. V. F., Mallmann, J. A. H., Schmidt, A. A., & Castañeda, H. O. 2000, A&A, 357, 621
Doublier, V., Caulet, A., & Comte, G. 1999, A&AS, 138, 213
Doublier, V., Caulet, A., & Comte, G. 2001, A&A, 367, 33
Dubinski, J., Mihos, J. C., & Hernquist, L. 1999, ApJ, 526, 607
Edmunds, M. G., & Pagel, B. E. J. 1984, MNRAS, 211, 507
Fabian, A. C. 1988, Hot Thin Plasmas in Astrophysics, 293, ed. R. Palavicini (Kluwer)
Ferland, G. J. 1996, HAZY, a brief introduction to Cloudy, University of Kentucky, Department of Physics and Astronomy Internal Report
Ferreras, I., & Silk, J. 2000, ApJ, 532, 193
Fioc, M., & Rocca-Volmerange, B. 2000 [astro-ph/9912179]
Gibson, B. K. 1997, MNRAS, 290, 471
Gondhalekar, P. M. 1986, Star Forming Galaxies and Related Objects, ed. D. Kunth, T. X. Thuan, & J. Tran Thanh Van (Edition Frontières, Gif sur Yvette), 145
Gordon, D., & Gottesman, S. T. 1981, AJ, 86, 161

Graham, A., Lauer, T. R., Colless, M., & Postman, M. 1996, ApJ, 465, 534
Grevesse, A., Noels, A., & Sauval, A. J. 1996, ASP Conf. Ser. 99, ed. S. S. Holt, & G. Sonneborn, ASP (San Francisco)
Heckman, T. M., Sembach, K. R., Meurer, G. R., et al. 2001, ApJ, 554, 102
Hunter, D. A., & Gallagher III, J. S. 1985, AJ, 90, 1457
Izotov, Y. I., & Thuan, T. X. 1999, ApJ, 511, 639
James, P. A. 1994, MNRAS, 269, 176
James, P. A., & Mobasher, B. 1999, MNRAS, 306, 199
King, I. 1966, AJ, 71, 64
Kunth, D., Maurogordato, S., & Vigroux, L. 1988, A&A, 204, 10
Kunth, D., & Östlin, G. 2000, A&ARv, 10, 1
Lake, G., Schommer, R. A., & van Gorkom, J. H. 1987, ApJ, 314, 57
Le Fèvre, O., Abraham, R., Lilly, S. J., et al. 2000, MNRAS, 311, 565
Lejeune, T., Cuisinier, F., & Buser, R. 1998, A&AS, 130, 65L
Lequeux, J., Kunth, D., Mas-Hesse, J. M., & Sargent, W. L. W. 1995, A&A, 301, 18
Lilly, S. J., Eales, S. A., Gear, W. K. P., et al. 1999, ApJ, 518, 641
Lisenfeld, U., Isaak, K. G., & Hills, R. 2000, MNRAS, 312, 433
Loose, H.-H., & Thuan, T. X. 1986a, in Star-forming dwarf galaxies and related objects, ed. D. Kunth, T. X. Thuan, & J. Tran Thanh Van (Éditions Frontières), p. 73
Mac Low, M.-M., & Ferrara, A. 1999, ApJ, 513, 142
Macchetto, F., Pastoriza, M., Caon, N., et al. 1996, A&AS, 120, 463
Martin, C. 1996, ApJ, 465, 680
Martin, C. L. 1997, ApJ, 491, 561
McGaugh, S. S. 1991, ApJ, 380, 140
McGaugh, S. S. 1994, ApJ, 426, 135
Madau, P., Ferguson, H. C., Dickinson, M. E., et al. 1996, MNRAS, 283, 1388
Marconi, G., Matteuci, F., & Tosi, M. 1994, MNRAS, 270, 35
Masegosa, J., Moles, M., & Campos-Aguilar, A. 1994, ApJ, 420, 576
Mendoza, C. 1983, Proc. IAU Symp., 103, 154
Mihos, J. C., McGaugh, S. S., & de Blok, W. J. G. 1997, ApJ, 477, L79
Meurer, G. R., Heckman, T. M., Leitherer, et al. 1995, AJ, 110, 2665
Östlin, G. 2000, Massive Star Clusters in Dwarf Starburst Galaxies, ed. A. Lancon, & C. Boily, ASP Conf., 211, 63
Östlin, G. 2000, ApJ, 535, L99
Östlin, G., & Kunth, D. 2001, A&A, 371, 429
Östlin, G., Bergvall, N., & Rönnback, J. 1998, A&A, 335, 85
Östlin, G., Amram, P., Masegosa, J., Bergvall, N., & Boulesteix, J. 1999, A&AS, 137, 419
Östlin, G., Amram, P., Bergvall, N., Masegosa, J., & Boulesteix, J. 2001, A&A, 374, 800
Pagel, B. E. J., Edmunds, M. G., Blackwell, D. E., Chun, M. S., & Smith, G. 1979, MNRAS, 193, 219
Pagel, B. E. J., Edmunds, M. G., & Smith, G. 1980, MNRAS, 193, 219
Pahre, M. A. 1999, ApJS, 124, 127
Papaderos, P., Loose, H.-H., Fricke, K. J., & Thuan, T. X. 1996, A&A, 314, 59
Raimann, D., Storchi-Bergmann, T., Bica, E., Melnick, J., & Schmitt, H. 2000, MNRAS, 316, 559
Rönnback, J., & Bergvall, N. 1994, A&AS, 108, 193
Sadler, E. M., Oosterloo, T. A., Morganti, R., & Karakas, A. 2000, AJ, 119, 1180
Sage, L. J., Salzer, J. J., Loose, H.-H., & Henkel, C. 1992, A&A, 265, 19
Salpeter, E. E. 1959, ApJ, 129, 608
Sandage, A., & Binggeli, B. 1984, AJ, 89, 919
Scalo, J. 1998, The Stellar Initial Mass Function (38th Herstmonceux Conference) ed. G. Gilmore, & D. Howell, ASP Conf. Ser., 142, 201
Searle, L., & Sargent, W. L. W. 1972, ApJ, 173, 25
Sersic, J. L. 1968, Atlas de Galaxias Australes, Cordoba, Argentina: Observatorio Astronomico
Silva, D. R., & Bothun, G. D. 1998, AJ, 116, 2793
Skillman, E. D. 1989, ApJ, 347, 883
Staveley-Smith, L., Davies, R. D., & Kinman, T. D. 1992, MNRAS, 258, 334
Stasińska, G. 1990, A&AS, 83, 501
Sung, E.-C., Han, C., Ryden, B. S., Chun, M.-S., & Kim, H.-L. 1998, ApJ, 499, 140
Taylor, C. L., Brinks, E., Pogge, R. W., & Skillman, E. D. 1994, AJ, 107, 971
Telles, E., & Terlevich, R. 1995, MNRAS, 275, 1
Terlevich, R., Melnick, J., Masegosa, J., Moles, M., & Copetti, V. E. 1991, A&AS, 91, 285
Thuan, T. X. 1983, ApJ, 268, 667
Thuan, T. X., & Izotov, Y. I., 1997, ApJ, 489, 623
Thuan, T. X., & Martin, G. E. 1981, ApJ, 247, 823
Thuan, T. X., & Seitzer, P. O. 1979, ApJ, 231, 680
Vila-Costas, M. B., & Edmunds, M. G. 1993, MNRAS, 265, 199
Vader, J., Patricia, F., Jay, A., Terndrup, D. M., & Heisler, C. A. 1993, AJ, 106, 1743
Worthey, G. 1994, ApJS, 95, 107
Zackrisson, E., Bergvall, N., Olofsson, K., & Siebert, A. 2001, A&A, 375, 814